THE INVESTIGATION OF STATIC AND DYNAMIC COMPRESSIVE DEFORMATION BEHAVIOR OF A PAPER BASED SANDWICH MATERIAL

A Thesis Submitted to
the Graduate School of
İzmir Institute of Technology
in Partial Fulfillment of the Requirements for the Degree of

MASTER OF SCIENCE

in Mechanical Engineering

by
Berkay Türkcan İMRAĞ

December 2022
İZMİR

ACKNOWLEDGMENTS

I would like to express my gratitude to Prof. Dr. Alper TAŞDEMİRCİ for his patience and guidance. This study would have never been accomplished without his inspiration and encouragement.

I would like to thank Bosch Termoteknik Manisa Plant R&D department for providing resources and support for this study.

I wish to thank to Panova Ambalaj San. Tic. A.Ş. for the specimens they provided

I would like to thank all of my friends at the IZTECH Dynamic Testing and Modelling Laboratory; Mesut BAYHAN, Mustafa Kemal SARIKAYA, Mehmet Kaan ZEYBEK, Samed ENSER, and Ayberk KARAKUŞ for their valuable support, and association.

I owe gratefulness to my colleagues at Bosch Termoteknik Manisa Plant R&D Department; İbrahim ŞİMŞEK, Çağatay KÖK, and Yiğit GÜRLER for their support..

I am deeply grateful to my parents for their financial and emotional support throughout my education life.

ABSTRACT

THE INVESTIGATION OF STATIC AND DYNAMIC COMPRESSIVE DEFORMATION BEHAVIOR OF A PAPER BASED SANDWICH MATERIAL

In this study, dynamic and quasi-static compression behavior of paper-based honeycomb sandwich structures were investigated. It is known that the mechanical properties of paper-based honeycomb structures change with changing strain rate values. For this reason, dynamic and quasi-static loading conditions should be considered separately when investigating the compressive behavior of the structure. In the material characterization studies, a series of tests were conducted to examine mechanical properties of the paper layer material and sandwich structure. Using data from mechanical tests, numerical models were established in the finite element tool LS-DYNA. Outputs of numerical models were validated with mechanical test outputs. After the validation study, the effects that influence the dynamic compressive behavior of the paper-based honeycomb sandwich structure and their contribution percentages were investigated using the opportunities provided by the FE tool. The results showed a 150.48 % difference between the dynamic and quasi-static compressive behavior of the structure. The numerical results obtained from explicit and implicit solvers also showed good correlation with the experimental results. In addition, the micro-mechanical modeling approach in numerical models made it possible to investigate the effects such as strain rate sensitivity of the paper layer material, entrapped air inside the core cells, and micro-inertia individually. The contribution percentages of the effects were calculated by comparing the numerical and experimental results.

ÖZET

KAĞIT ESASLI SANDVİÇ MALZEMENİN STATİK VE DİNAMİK BASMA DEFORMASYON DAVRANIŞININ İNCELENMESİ

Bu çalışmada, kağıt esaslı petek sandviç yapıların dinamik ve yarı statik bası davranışı incelenmiştir. Kağıt esaslı petek sandviç yapıların mekanik özelliklerinin değişen gerinim oranı değerleri ile birlikte değiştiği bilinmektedir. Bu nedenle, yapının bası davranışının incelenmesinde dinamik ve yarı statik yükleme durumları ayrı ayrı ele alınmalıdır. Malzeme karakterizasyonu çalışmalarında, kağıt esaslı malzemenin ve sandviç yapının mekanik özelliklerinin incelenmesi için bir dizi test gerçekleştirilmiştir. Mekanik testlerden elde edilen veriler kullanılarak LS-DYNA sonlu elemanlar analiz programında nümerik modeller kurulmuştur. Kurulan nümerik modellerden elde edilen çıktılar, mekanik testlerden elde edilen çıktılar ile doğrulanmıştır. Doğrulama çalışmasının ardından kağıt esaslı petek sandviç yapıların dinamik bası davranışına tesir eden etkiler ve bu etkilerin katkı yüzdeleri sonlu elamanlar aracının sağlamış olduğu olanaklar kullanılarak incelenmiştir. Sonuçlar yapının dinamik ve yarı statik bası davranışı arasında %150.48' lik bir fark olduğunu göstermiştir. Ayrıca implicit ve explicit çözücülerden elde edilen nümerik sonuçlar da deneysel sonuçlarla iyi bir kolerasyon ortaya koymuştur. Ek olarak nümerik modellerde izlenen mikro mekanik modelleme yaklaşımı, hücre duvarının gerinim oranı duyarlılığı, hücre içerisinde hapsolmuş hava ve mikro atalet gibi etkilerin ayrı ayrı incelenmesini mümkün kılmıştır. Nümerik ve deneysel sonuçların karşılaştırılması ile bu etkilerin katkı yüzdeleri hesaplanmıştır.

TABLE OF CONTENTS

LIST OF FIGURES

Figure **Page**

Figure **Page**

Figure **Page**

LIST OF TABLES

LIST OF SYMBOLS AND ABBREVIATIONS

σ	Stress
ρ_{pk}	Peak Stress
ρ_{pl}	Plateau Stress
ε	Strain
ε_D	Densification Strain
ρ	Density of the Paper-Based Material
ρ_m	Density of Honeycomb Core
ν	Poisson's Ratio
E	Elastic Modulus
t	Thickness of Cell Wall/Face Layer
l	Length of Single Cell Wall
k	Length of Double Cell Wall
θ	Cell Expansion Angle
V	Cross Head Velocity
L	Gauge Length
m	Nodal Mass
t	Time
c	Cowper-Symonds Equation Constant
p	Cowper-Symonds Equation Constant
FE	Finite Element
FEM	Finite Element Method
RH	Relative Humidity
DIT	Direct Impact Test
ASTM	American Society for Testing and Materials
MD	Machine Direction
CD	Cross Direction

CHAPTER 1

INTRODUCTION

Due to their lightweight, relatively high strength, good energy absorption properties, cost-effectiveness, and recyclability paper-based honeycomb sandwich materials have been mostly used as a packaging and filling material in various industries. Paper-based honeycomb sandwich materials provide a considerable amount of energy absorption. The energy absorber materials must have the best impact energy absorption capabilities while having the lowest density possible. To absorb the impact energy, a sandwich structure is constructed using various lightweight materials (wood, paper, polymers, fabrics, and composites) with various geometric designs. To improve energy absorption capacity at relatively low weights, conventional or bio-inspired geometric patterns (corrugated, honeycomb, re-entrant, diamond, and truss) are used in the design of sandwich structures. However, sandwich structures show different mechanical behaviors under different loads depending on the type of core and core material they have. Therefore, material characterization and numerical modeling studies should be carried out to predict how the sandwich structures will perform in the different applications in which they will be used. Due to environmentally friendly regulations prepared by governments, paper-based honeycomb sandwich materials and other environmentally friendly material alternatives are becoming more important.

1.1. Fundamentals of Energy Dissipation

The use of energy-dissipating materials aims to provide packaged goods the most protection against loading situations that are higher than usual. These materials dissipate the kinetic energy generated during impact to limit the magnitude of the energy transmitted to a packaged item. Energy-dissipating materials dissipate energy by acting like viscous non-linear springs. Energy dissipation is usually provided by plastic deformation of the energy-dissipating material. However, at some point, the ability to

dissipate energy is lost depending on the material property, geometric parameters, or porosity. This point is known as the densification strain [5].

In Figure 1.1. and 1.2., stress-strain curves of expanded polystyrene and paper-based honeycomb materials under compressive load are shown.

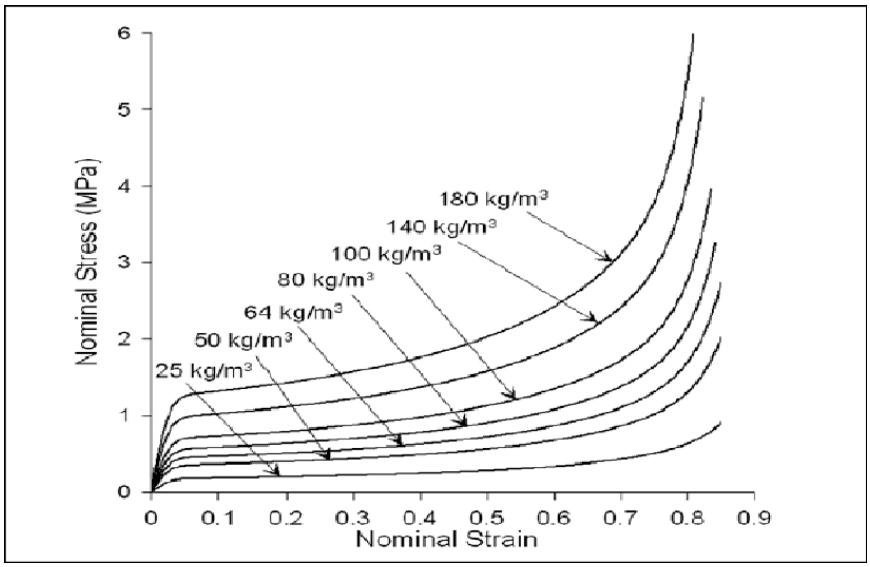

Figure 1.1. Stress-strain curve of EPS with different densities [4].

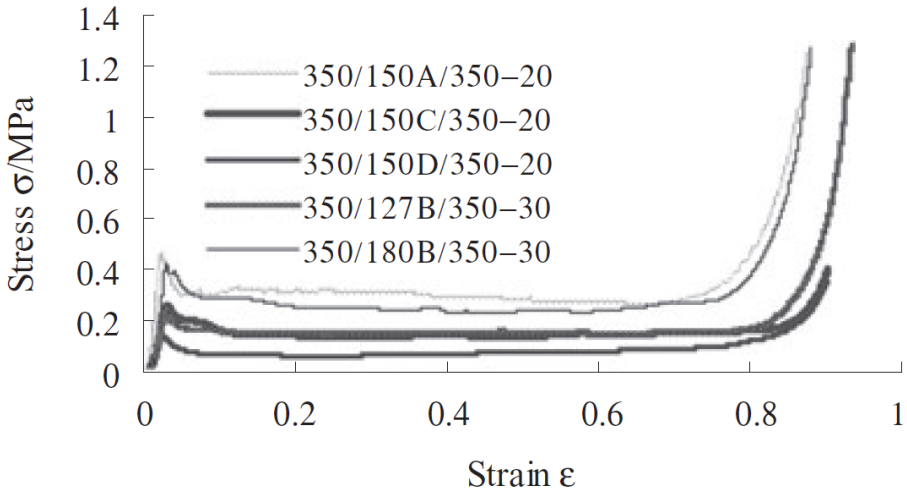

Figure 1.2. Stress-strain curve of paper-based honeycomb with different core types [6].

As mentioned above, the energy-dissipating material design aims to dissipate the kinetic energy at a tolerable level. Therefore, some design approaches can be applied to create an effective material. These basic design preferences are: Providing steady

deformation mode, irreversible energy conversion, relatively high specific energy absorption capacity, extended stroke, being lightweight and cost-effective [3].

1.2. Literature Review

1.2.1. Bio-Inspired Design

Biological-based designs are mentioned in many studies that offer innovative and effective solutions in engineering applications. Remarkable results in this research field have made the subject of bio-inspired design even more attractive recently. Biomimicry is a field of research that draws its inspiration from natural systems and models [1]. In the 1960s, the concept of biomimicry (greek words for life and to copy are bio- and -nimesis.) was introduced in literature and became famous in the 1980s [1,7]. According to this concept, billions of years of natural evolution should guide innovations [34]. We should take an approach that nature is a guide and a source of inspiration, and providing sustainability should be primary goal of this approach. [2]. The main aim in the bio-inspired design approach is to discover a unique structure from nature and apply it to engineering designs.

In the study published by Tasdemirci et. al. [8], the dynamic and quasi-static compressive response of a sandwich structure consisting of balanus-shaped cores was examined with experimental and numerical methods. The compression test models of balanus structure, which were run at quasi-static and dynamic strain rates, showed good agreement with the experimental results.

Figure 1.3. Balanus, Balanus-shaped core sandwich structure specimen and FE model [8].

Aizenberg et al. investigated the skeletal structure of Euplectella and concluded that the skeletal structure provides attractive structural stability. Due to the advantages of this skeletal structure, it can be found in the supporting system models of high-rise buildings such as skyscrapers [9].

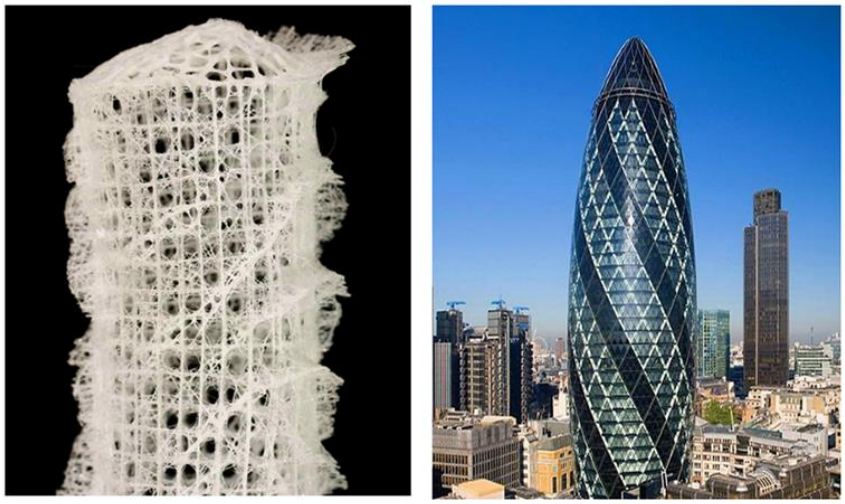

Figure 1.4. Implementation of the Euplectella structure in skyscraper construction [9].

1.2.3. Quasi-Static and Dynamic Crushing Behavior of Paper-Based Honeycomb Structures

A paper-based honeycomb structure has three components: two faces and a cellular honeycomb core (top and bottom). Both the faces and the core are produced from various types of paper-based material. Glue is used to bind faces to top and bottom core ends. Paper strips are bonded with glue to create the honeycomb core. There are two double-thickness (2t) cell walls and four single-thickness cell walls in each hexagonal core cell. A cell wall length is shown by the "l". Adhesive layer thickness between the double-thickness cell walls is neglected.

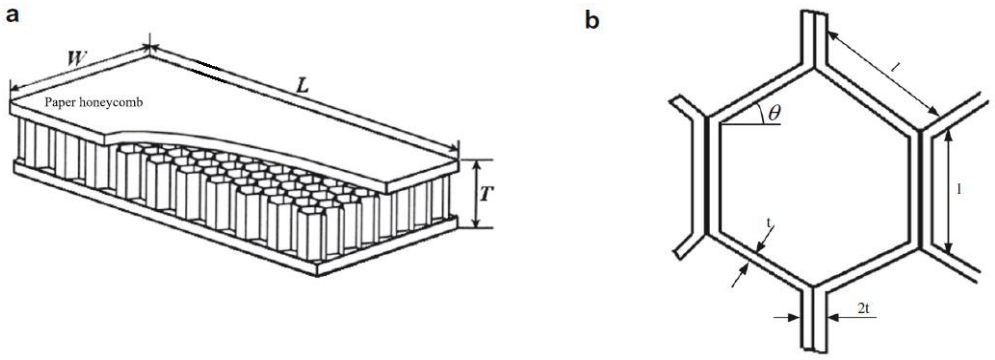

Figure 1.5. Geometric parameters of paper-based honeycomb sandwich structure and unit core cell [10].

In the use of paper-based honeycomb sandwiches as packaging elements, the structure provides protection to the goods by behaving as a nonlinear spring. This structure disperses the impact over a longer period of time, reducing the transmitted peak force and absorbing kinetic energy by folding the cell walls, reducing the overall effect of impact [5].

Regardless of the wall material, honeycomb structures have a typical stress-strain curve under the applied compressive load in the through-thickness direction. There are four phases in this curve: linear elastic region, elastic-plasticity (pre-plateau) region, plasticity collapse (plateau) region, and densification region [11].

1. Linear elastic region: The stress-strain curve is linear. No plastic deformation is observed.
2. Elastic-plasticity region: It is the phase in which the first plastic deformation (folding) is observed in the honeycomb core. After this phase, the initial form of the honeycomb sandwich structure changes irreversibly.
3. Plasticity collapse region: As the compression strain increases until all of the core walls are folded, stress values seem to fluctuate. This phase is also called the plateau phase.
4. Densification region: The compressive stress values increases rapidly when strain values passes the densification region, the paper-based honeycomb nearly lost its elastic properties. After this point, the structure has lost its ability to absorb energy.

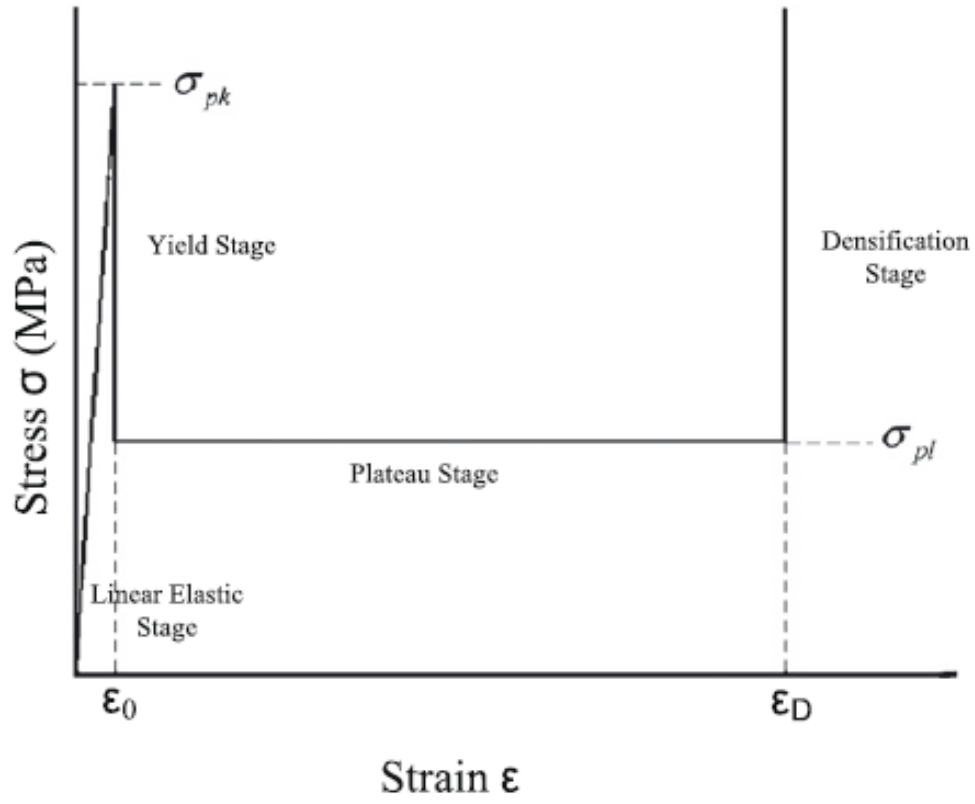

Figure 1.6. Simplified stress-strain curve of paper-based honeycombs under compressive load in the through-thickness direction [10].

Three points are important in terms of evaluating the stress-strain curve of honeycomb structures: peak stress, which occurs in stiffest form of the honeycomb structure before folding of the cell walls, stiffest form; plateau stress, determined by the stress values resulting from the propagation of the folding deformation and the densification strain that occurs when all the cell walls are folded.

Most of the research on the crushing behavior of paper-based honeycombs has focused on the quasi-static compressive behavior. Aminanda et al. [14] revealed that paper-based honeycombs exhibit quasi-static axial compressive behavior that is similar to honeycombs made of nomex and aluminum.

Lu et. al. [12] developed mathematical methods to investigate the required buckling load for the delamination of glued cell walls and collapsing limit of the structure under axial compressive load. They validated their models by comparing the models and the results of the crush test performed at 10 mm/min. The comparison showed that the mathematical models have a close correlation with the test results. Detailed material or geometric parameter information is not given for the paper-based honeycomb specimens

used in the experimental studies. The findings of their studies were shown as a critical buckling load vs stretching ratio (degree of core wall expansion) graph in Figure 1.7.

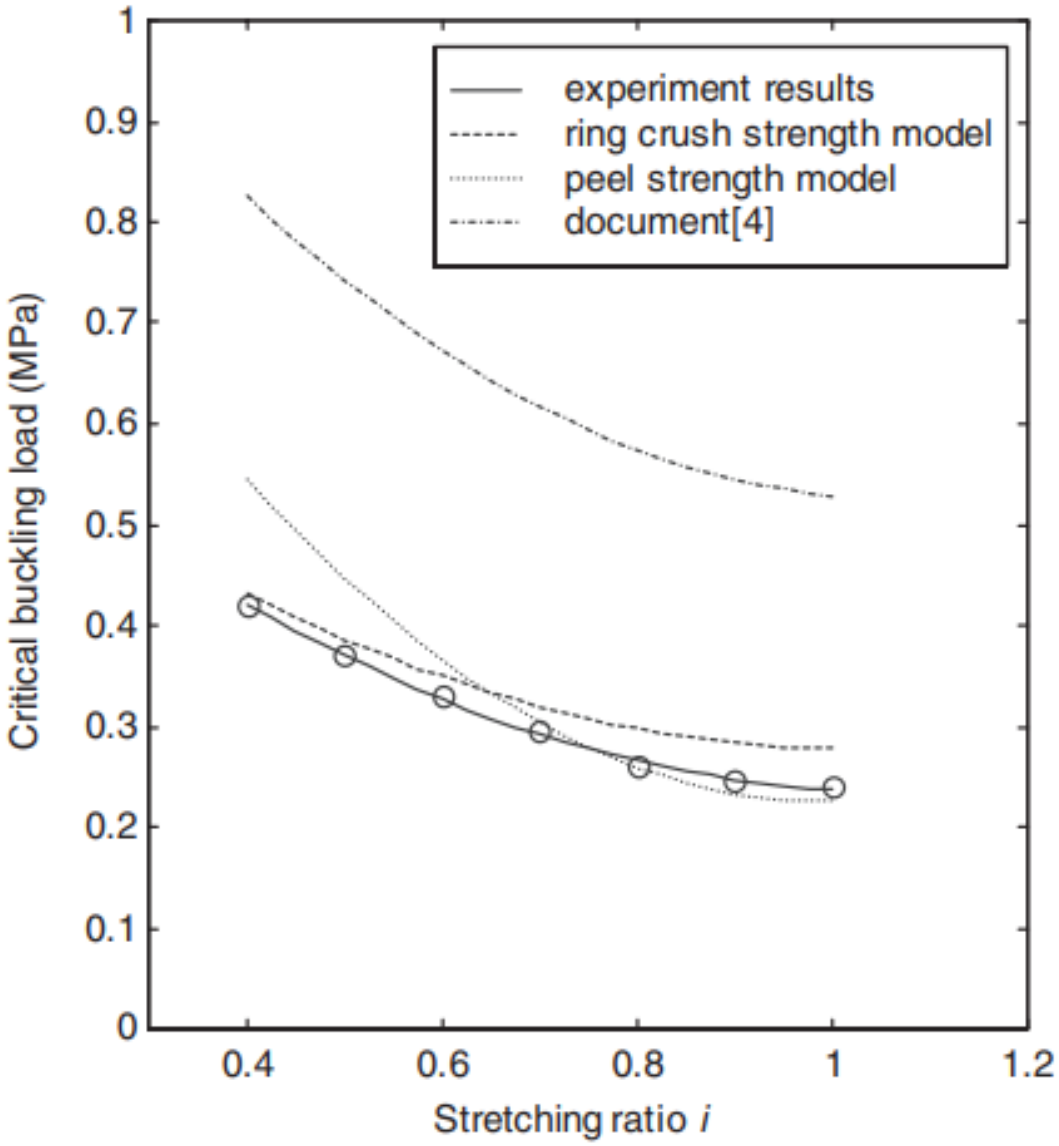

Figure 1.7. Critical buckling load vs. stretching ratio [12].

Wang et al. [13] studied on the effect of paper-based honeycombs with different geometric parameters on the quasi-static compressive behavior under 12 ± 2 mm/min constant displacement velocity. The examined geometric parameters were core height ranging from 10mm to 50mm, basis weight of paper-based material ranging from 112 to 180 g/m^2, cell wall layer thickness between 0.2 and 0.29 mm, and diameter of cells ranging from 5.8 to 14.4 mm. In addition, the effect of bottom and top faces and the compressive behavior of the combined structures containing more than one honeycomb

layer were investigated. The specimens investigating in the tests have a planform area of 200 x 200 mm. The tests were performed at a controlled condition of 23°C and 50% RH. [6].

The main findings in the published figures, the strength of the paper-based honeycomb structure with faces is higher than that of the honeycomb structure without faces, despite the similarity in the stress-strain curves of the two types of honeycomb structure. It was concluded that the stress values especially in the plateau region were quite different. However, the study published by Côté et al. [44] shows that the compressive behavior of metallic honeycombs with and without faces does not affect as much as paper-based honeycombs. For this reason, while the effect of faces can be neglected in metallic honeycombs under certain conditions, this effect should be considered in paper-based honeycomb.

Geometric parameters such as paper layer thickness, wall length, and cell diameter were examined as core design variables in the calculation of relative density. An average paper-based honeycomb density can be calculated with the average density of the face and the cell wall materials. When this average paper-based honeycomb density was compared with the energy absorption capacity, no significant trend was found, although there were differences between the results.

Equation 1.1 was used for the relative density calculation.

$$\frac{\rho_m}{\rho} = \left(\frac{t}{l}\right) \frac{1 + {}^{k}/_{l}}{\left({}^{k}/_{l} + sin\theta\right)cos\theta} \tag{1.1}$$

where ρ_m is the density of paper-based core; ρ is the density of the paper-based material, k is the length of the double-thickness cell wall, t is the thickness of paper layer, l is the length of the single-thickness cell wall, and θ is the cell expansion angle.

Investigated were the effects of core height and a double-layer structure on the amount of energy absorbed per volume, these geometric variations appeared to affect the compression behavior, but no significant correlation was observed. Tests were carried out with specimens which have different cell wall thicknesses, but no direct comparison was

published between the compressive behavior of specimens. According to Wang et al., cell wall thickness increases core stiffness.

In the study published by Wang et al. [15], the energy absorption capability of paper-based honeycombs at quasi-static strain rates were investigated. Specimens with various cell wall t/l ratios were used in the study. Its macroscopic compressive behavior was investigated in order to develop an analytical approach for the energy absorption of paper-based honeycombs. It was seen that there was a good correlation between the values obtained using the mathematical model and the results of the experiments. When the results were examined, it was found that a higher cell wall t/l ratio increases the energy per unit volume.

E et al. [16] investigated the effect of relative humidity on the crushing behavior of paper honeycomb structures. Specimens with different core diameters but the same wall thickness and planform area were used in the experimental studies. Specimens were conditioned at relative humidity values ranging from 40 % to 95 %. Constant velocity is 12 ± 3 mm/min. It was seen that 75% RH value is the required threshold value for the paper honeycomb to have a remarkable effect on the energy absorption. There was a rapid decrease in energy absorption for RH values above 75%, which was proportionally greater for higher cell wall t/l ratios. Significant changes were observed in the plateau region due to humidity.

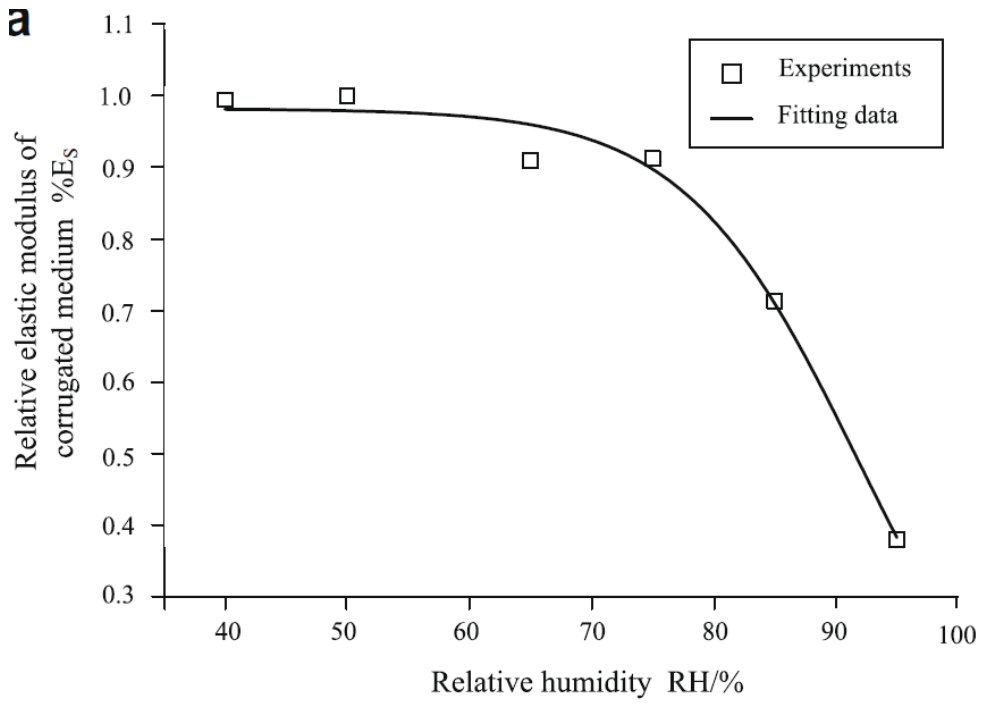

Figure 1.8. Relative elastic modulus vs. relative humidity [16].

In the study published by J. Reay [5], it was stated that at quasi-static strain rates, the entrapped air in the honeycomb cells had significantly more time to be evacuated from the permeable paper-based structure. As a result, the internal entrapped air pressure is negligible compared to the structural response. The function of the structure has a significant effect on the quasi-static compressive behavior of paper-based honeycombs. However, it is known that the entrapped air pressure in the core cells affects the results in dynamic loading situations. Therefore, the dynamic compressive behavior of paper-based honeycombs needs to be considered individually.

Wu et. al. [17] examined the quasi-static and dynamic compressive behavior of 5056 and 5052 aluminum honeycombs of different core dimensions up to test velocities of 25 m/s. Researchers observed that the thinner aluminum honeycomb specimens, with smaller cell size and stronger core material cause greater energy absorbtion in the loading direction.

Zhao and Gary [18] investigated the compressive behavior of aluminum honeycombs at dynamic strain rates. The Split Hopkinson Pressure Bar test setup, which generated impact velocities ranging from 2 m/s to 28 m/s, was used to test aluminum honeycomb specimens. As a result of the research, it was observed that the average crushing strength of the specimens increased by as much as 40%.

Using a similar test system, Zhao, Elnasri, and Abdennadher [19] performed quasi-static and dynamic (10 m/s) axial compression tests for 5056 and 5052 aluminum honeycombs with various core types. Depending on the type of specimen used, the test results revealed a hardening between the quasi-static and dynamic responses of between 12% and 25%. The researchers ignored the effect of entrapped air to determine the main reason of high-strain rate hardening and concluded that the hardening is in part due to the strain rate sensitivity of aluminum. However, they reported that the major effect on stiffness was micro-inertia.

Yamashita and Gotoh [20] investigated the compressive behavior of 5052 aluminum honeycomb specimens at low and high strain rates. They concluded that the stress value at plateau region increases with increasing strain rate under dynamic loading, while the stress value at plateau region is relatively flat during quasi-static compression. According to their findings, the strain rate sensitivity of core layer material, micro-inertia, and entrapped air inside the cells are the causes of the strain rate dependent stiffening on the plateau region. The researchers observed that the difference in plateau stress values between the quasi-static and dynamic test results was roughly 50%.

Energy-dissipating material alternatives were investigated by Smithson [21] for use in airdrop aid packages. Impact tests were performed on the candidate material alternatives examined in the study. Paper-based honeycomb materials were found to be remarkable among the candidates due to their energy absorption ability, lightweight, and cost-effectiveness. Specimens with 610 mm diameter and various core heights from two different manufacturers were conditioned at specific relative humidity values. Paper-based honeycomb specimens were examined at impact velocity values ranging from 4.5 m/s to 15 m/s. The energy absorption capacities of the paper-based honeycomb specimens were measured in the 240 kJ/m^3 to 410 kJ/m^3 range. It was seen that the energy absorption ability of the specimens decreased with increasing relative humidity and core height increased with increasing impact velocity.

In another study by Ripperger and Briggs [22,23], the crushing strength of paper-based honeycombs and the effect of internal air pressure on them were investigated. Impact tests were carried out at velocities varying between 6.2 m/s and 6.7 m/s. Ripperger and Briggs concluded that at low strain rates, the compressive strength of paper-based honeycomb is mainly affected by geometric parameters, and at higher strain rates, the compressive strength is mainly affected by the entrapped air in the core cells. However, they expanded their work to study this entrapped air effect.

In the extended study of Ripperger and Briggs focused on four different test scenarios.

1. Testing specimens with top and bottom faces to seal air in core cells and without top and bottom faces to allow entrapped air in core cells to evacuate.
2. Testing rectangular specimens with the ribbon direction orthogonal and parallel to the long side.
3. Testing samples using plastic faces instead of paper-based faces.
4. Performing burst test of custom constructed unit cells with nitrogen gas.

As a result of the study, the following results were observed:

1. Specimens with faces were roughly 15% stiffer due to the effect of air trapped inside the cell, the post-test structure was more deformed, and delamination was observed between the adhesive applied double-layered cell walls.
2. It was seen that the ribbon direction had little effect in the early crushing stage, However, in the later crushing stages, honeycomb specimens with ribbon direction oriented parallel to the long edge were exhibit a stiffer behavior.

3. It was observed that extra sealing was provided to the specimens with plastic bags. Modified specimens absorbed 10% more energy on average than those without additionally sealed.
4. In the burst tests, single-core cells burst at roughly 34.4 kPa and delamination occurred at the adhesive-applied double-layered core walls.

Ripperger and Briggs [22,23] concluded that internal entrapped air pressure could increase the energy absorption ability depending on the number of air-filled cells in the planform area and their sealing status, but it could decrease the energy absorption ability if the entrapped air could be escaped easily.

Guo et. al. [24] performed drop test series to obtain the cushioning curves of paper-based honeycombs for various core thicknesses. Within the scope of their studies they created cushioning curves. Those curves represent the relationship between the maximum deceleration (y-axis) an protected item is subjected to and the static stress (x-axis) caused by the weight of the protected item. Cushioning curves from the drop tests are concave and upwards facing. The limit where the paper-based honeycomb packaging elements provide the most protection is indicated by the lowest acceleration value in the cushioning curve. It was found that the concavity and peak acceleration values of the paper-based honeycomb cushioning curves decreased as the core thickness increased. That means that thicker honeycombs provide greater energy absorption over a wider range of static stress values.

Another study published by Wang [25] examined the effects of cell diameter selection, paper layer thickness, and core height on the dynamic compressive behavior of the paper-based honeycomb sandwich structure. The results showed that as cell diameter increased, energy absorption per unit volume decreased, and a fluctuating but in general favorable relationship between height of core and energy absorbed per unit volume. The cushioning curves obtained in Wang's study are similar to the curves published in the study by Guo and Zhang [24]. In both studies, the effect of entrapped air pressure in the core cells was not examined individually.

A study has been published by J.Reay [5] to investigate the dynamic energy dissipation capabilities of paper-based honeycombs. In this study, specially produced specimens with three different core types were used. All paper-based honeycomb specimens were 70 mm in core thickness and 250 x 250 mm in the planform area. The

specimens were examined at impact velocities ranging from 5 m/s to 6.5 m/s in the gas gun test setup prepared for the examination of the dynamic response.

As a result of the experimental study, the following results were observed:

1. As the cell diameter decreases, the cell numbers in the planform area increases. Paper-based honeycombs with finer cells exhibit stiffer compressive behavior.
2. Increasing the planform area of the honeycomb specimens increases the peak and plateau stress values.
3. Depending on the impact velocity, as the increase on the initial peak stress, there was evidence of some strain rate sensitivity.
4. At low strain rates, the internal air pressure had little or no effect on the compressive behavior of the sandwich structure. At low strain rates, the compressive behavior is changed by the material type and the geometrical parameters of the core.

After the experimental studies, J.Reay developed an effective numerical modeling approach for honeycomb structures by using FEA tools to investigate the sub-effects on compressive behavior. In the numerical model developed by J.Reay, the material card input values taken from the literature were used for the mechanical properties of the kraftliner material. The material properties taken from the literature were optimized by using FEA tools and converged to the results obtained from the dynamic tests of honeycomb specimens. In J. Reay's micro-mechanical model, effects such as element size, entrapped air, and adhesive strength were investigated individually.

The main findings of the numerical modeling study:

1. Energy absorption per unit volume of paper-based honeycomb structures increases with increasing elastic modulus, yield strength, tangent modulus, wall thickness, and the number of whole cells in the planform area. Adhesive strength, core height, , and cell wall length also affect the energy absorption per unit volume.
2. Energy absorption per unit volume of paper-based honeycomb structures increases with increasing elastic modulus, yield strength, tangent modulus (post-yielding), wall thickness, and the complete cell number in the

planform area. Adhesive strength, length of cell wall, and core height also affect the ability to absorb energy per unit.

In the material model of kraftliner, strain rate sensitivity and orthotrophy of the kraftliner are neglected.

In addition to the studies performed to investigate the mechanical behavior of paper-based honeycombs, studies have also been carried out to investigate the mechanical properties of paper types used as cell wall materials. Paper is inherently a material that varies in fiber orientation and mechanical properties. The raw material from which paper-based materials are produced determines their mechanical properties, and the pulp may contain recycled pulp. The amount of recycled pulp in the paper can be interpreted by examining the virgin fiber ratio. Its characteristics depend on the paper type from which it is produced, and the pulp may contain recycled pulp. The amount of recycled pulp in the paper can be interpreted by examining the virgin fiber ratio. In addition, the pulp is a natural material, so its chemical and mechanical properties may vary depending on the growing conditions of the plant from which it is produced. Many studies have been carried out to determine the mechanical properties of various commercial paper types, which are widely used in the packaging and printing industry.

In the study published by Baum et al. [26]. The elastic modulus, shear modulus, and poisson's ratio of a kraftliner were characterized by investigating its acoustic response in each fiber orientation (MD&CD). However, this material characterization method is only applicable to the measurement of paper properties in the elastic region. This means that the method is valid only for quite small strains.

In the production process, paper materials are rolled. The fibers are aligned in the rolling direction during the rolling process. This direction is known as the machine direction (MD) in the literature. The fiber orientation orthogonal to the rolling direction is known as the cross direction (CD). The fiber alignment of paper-based material makes it stronger and stiffer in the machine direction compared to the cross direction.

Mäkelä et. al. [27] studied on to develop an analytical orthotropic elastic-plastic constitutive paper model that can be calibrated by tensile tests in three directions. This model can be used to predict static anisotropic stress-strain behavior for fiber directions between machine and cross direction.

In the publication by Castro et. al. [28], a constitutive model is developed for the biaxial tension behavior of the paper. This model takes into account the elastic-plastic

hardening behavior and orthotropic character. The developed model considers the elastic-plastic hardening and orthotropic behavior. Typical stress-strain curves for the machine and cross directions given by the researchers are shown in Figure 1.9.

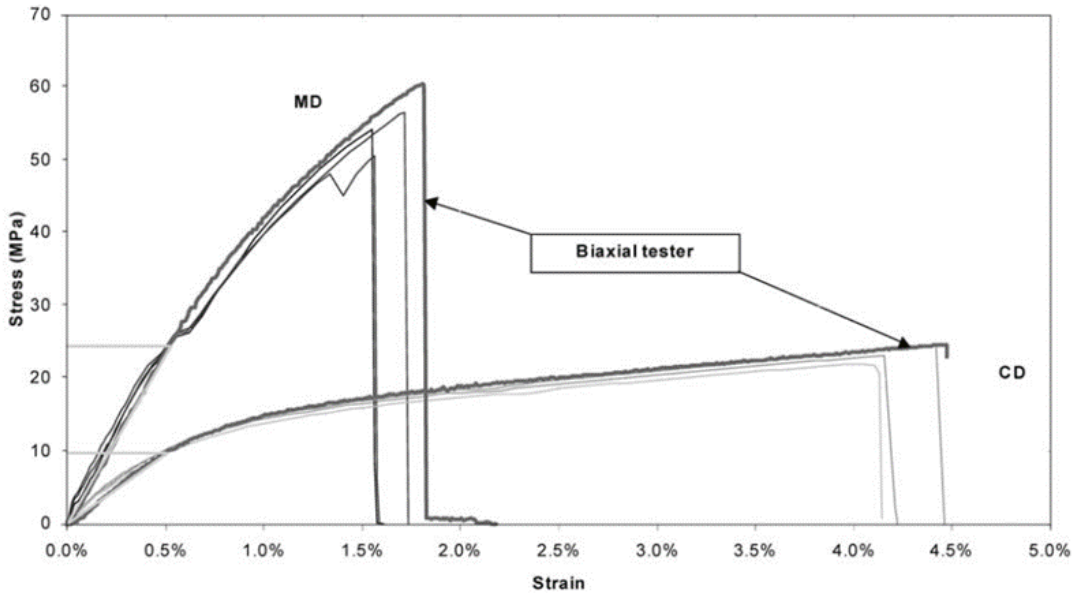

Figure 1.9. Stress–strain curves in uniaxial loadings in machine and cross direction [28].

Allaoui et al. [29] stated that the paper undergoes plastic deformation when subjected to cyclic load. They have also stated that the plastic deformation of the paper is dependent on the strain rate, a hardening effect becomes significant when the strain rate is increased from 6 x 10^{-5} s^{-1} to 12 x 10^{-3} s^{-1}.

In the study published by Godshall [30], the test setup developed to investigate the dynamic stress-strain relationship of paper materials was explained. With the developed test setup, specimens prepared from two different paper types were examined at strain rates from 50 x 10^{-5} s^{-1} to 50 s^{-1}. Specimens were prepared in MD vs CD directions considering fiber directions. As a result of the study, it was observed that the papers were strain rate sensitive and exhibited parabolic strain hardening.

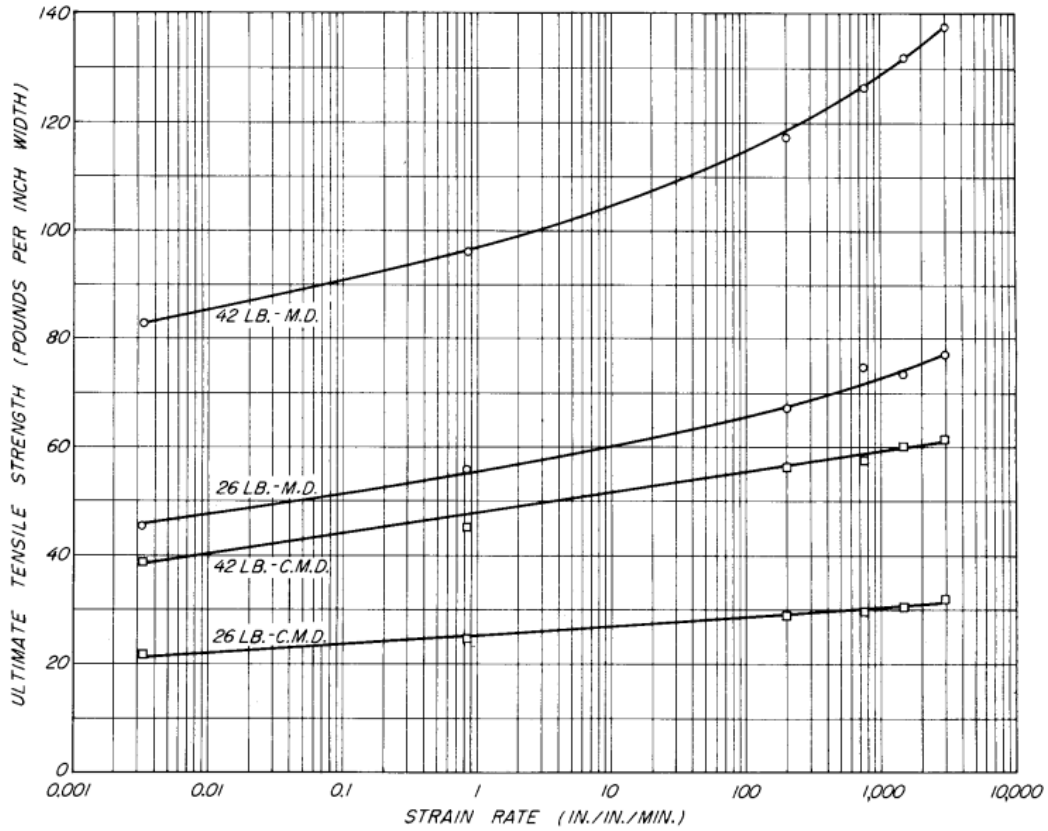

Figure 1.10. Comparison of strength characteristics for two weights of kraftliner [30].

1.3. Thesis Objective

The scope of this study is to investigate dynamic and quasi-static compressive behavior of paper-based honeycomb sandwich structures, which is an environmentally friendly material. In order to achieve this aim, material characterization of honeycomb specimens was carried out under dynamic and quasi-static loading conditions. However, data from mechanical tests are limited due to the current measurement methods. For this reason, the finite element tool LS-Dyna was used to obtain more detailed data about the compressive behavior of the honeycomb sandwich structure.

In the literature review, it was found that the main effects on the dynamic compressive behavior of honeycomb structures are strain rate sensitivity of paper layer material, entrapped air in core cells and micro-inertia. While these effects are negligible in the quasi-static loading cases, they cannot be neglected in the dynamic loading cases. For this reason, it is a requirement that the numerical modeling approach to be chosen can simulate these effects. When the Ls-Dyna theory manual and similar studies in the

literature are examined, it is concluded that the most feasible approach for numerical models is micro-mechanical modeling. Therefore, a proper material model that can be used in numerical models was selected and an adequate mesh model for honeycomb structure was established with 2D shell elements.

The results from mechanical tests which are performed under the same boundary conditions were used to validation of numerical models. The numerical results showed good correlation with the experimental results. After the validation study, the conditions in the numerical models were changed and the contribution percentages of the effects which are contributing to the dynamic compressive behavior of the paper-based honeycomb sandwich structures were calculated.

CHAPTER 2

MATERIALS AND METHODS

In this section, material characterization methods for investigating the mechanical properties of krafliner paper and honeycomb structure are explained. The data obtained from the characterization study were used in both material model development and validation studies. Since kraftliner material and honeycomb sandwich structure are strain rate sensitive, dynamic testing at high strain rates is as important as quasi-static testing in mechanical characterization. While there are valid test standards for quasi-static test methods, custom test setup is used for dynamic test methods.

2.1. Specimen Selection and Preparation

Three types of specimens were used in this study. The first of these specimen types is the paper strip specimens prepared to obtain the mechanical properties of kraftliner paper. Paper strip specimens prepared for the tensile test were prepared in accordance with the ASTM D828-16 [34] standard. The prepared tensile test specimens have a width of 25.4 mm, a length of 100 mm, and a thickness of 0.28 mm. Paper strip tensile test specimens were prepared orthogonal to the fiber directions (CD) and parallel to the fiber directions (MD), considering the paper fiber alignment. The primary objective of this process is to investigate the change in mechanical properties of kraft liner paper material due to orthotropy.

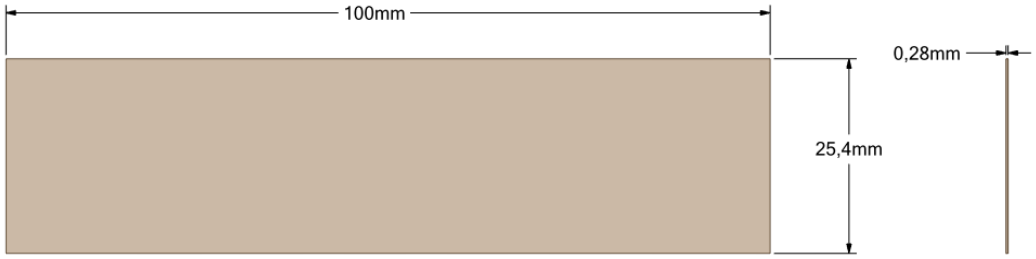

Figure 2.1. Dimensions of Paper Strip Specimen

The second specimen type is 50mm x 50mm square specimens made of kraftliner paper used in quasi-static compression tests. Square specimens prepared for quasi-static

compression tests were prepared in accordance with ASTM C365 / C365M – 16 [35] standard.

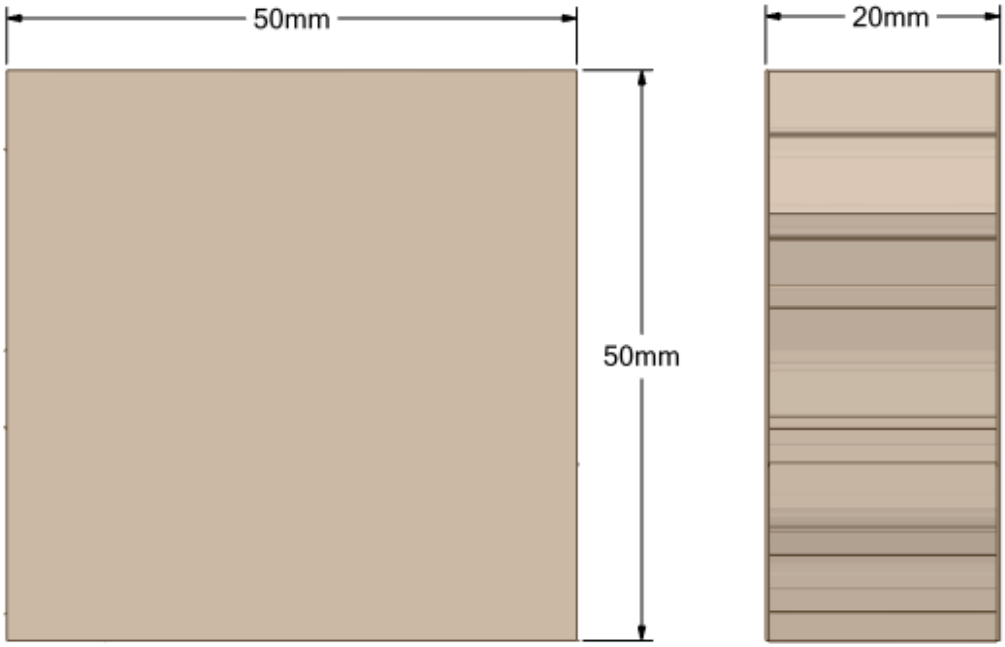

Figure 2.2. Dimensions of Square Honeycomb Sandwich Structure Specimen

The last specimen type is circular specimens with a diameter of 40mm, which are also made of kraftliner paper for dynamic compression tests. There is no ISO or ASTM standard for dynamic compression test. The specimens were prepared in accordance with the striker bar diameter.

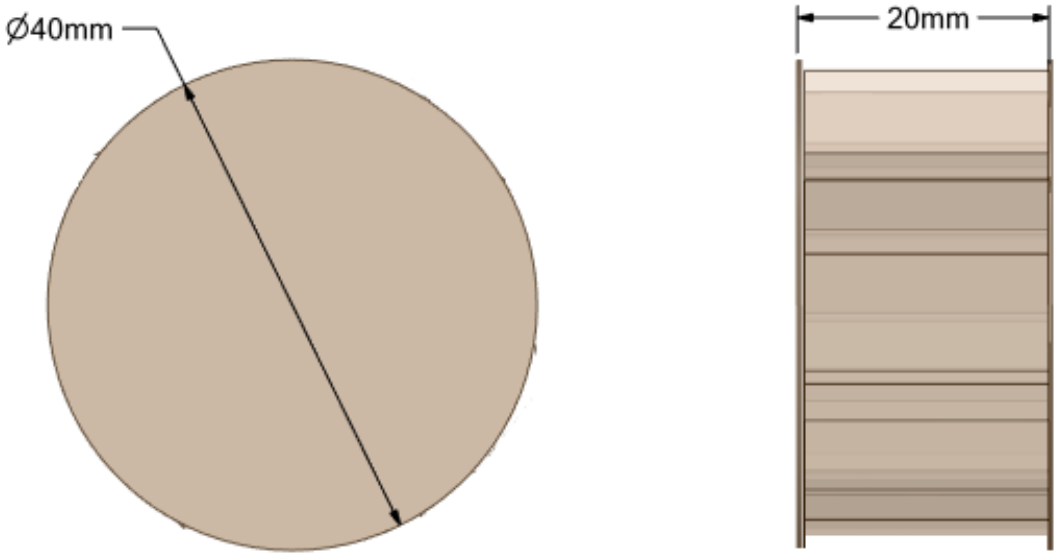

Figure 2.3. Dimensions of Circular Honeycomb Sandwich Structure Specimen

In the ideal case, the core of the sandwich structure should consist of regular shaped hexagons. However, due to the production method, imperfections occur in the core structure of the products. For this reason, all specimens used in compression tests were extracted from honeycomb panels produced on the same production line.

2.2. Material Characterization and Crushing Tests

This section provides details about the procedures followed in the characterization study. The characterization study was carried out for two main objectives:

1) Fiber alignment dependent mechanical behavior of kraftliner material.
2) Characterization of strain rate dependent behavior of paper-based honeycomb sandwich structure.

2.2.1 Quasi-Static Tests

The quasi-static testing of the materials was done first because it is less laborious than the custom dynamic testing setups and provides the deformation history that can be obtained through the testing machine software. During the quasi-static tests, the load and displacement were continuously monitored for detailed observations about the quasi-static deformation mechanism of the paper strip and honeycomb sandwich specimens. The most preferable method to investigate the deformation behavior at low strain rates is to carry out a quasi-static test on specimens of known gauge length and cross-sectional area. The stress-strain curve of the paper strip specimens examines in two different regions as elastic and plastic. However, this approach is different for honeycomb sandwich structures. Honeycomb sandwich structures usually have a unique stress-strain curve characteristic, regardless of the material from which they are made. This unique stress-strain curve is examined in three different regions as linear elasticity, plateau, and densification.

2.2.1.1. Tensile Test of Paper Strip Specimens

In this experimental study, a material characterization study was carried out for kraftliner type paper material, which is widely used in the production of paper-based sandwich structure packaging materials. In the characterization study, both fiber directions called MD and CD were taken into account. The obtained characterization data were used in the development of material cards for the numerical modeling study. Tensile test specimens have a width of 25.4 mm, a length of 100 mm, and a thickness of 0.28 mm. During the tests, the gauge length was measured as 50 mm.

A uniaxial tensile test was conducted for material characterization of kraftliner paper strip specimens. Quasi-static tensile tests were performed with Shimadzu AG-X universal testing machine. The Shimadzu AG-X universal testing machine allows for performing quasi-static tests at various strain rates ranging from 10^{-4} s^{-1} to 10^{0} s^{-1}.

Figure 2.4. Shimadzu AG-X universal testing machine.

A video extensometer was used to trace and measure the displacement of markers placed on the chins. Displacement measurements were made with this video extensometer to improve measurement accuracy. In addition, the video extensometer was recorded until the end of the test to observe the deformation mode. During the tensile test, a quasi-static

strain rate of 10^{-3} s^{-1} was applied. To observe the anisotropic behavior, uniaxial tensile tests were repeated twice for two different specimen types prepared in the MD and CD directions.

2.2.1.2. Compression Test of Paper Honeycomb Sandwich Specimens

In this section, test setups prepared to investigate the compressive behavior of paper-based honeycomb sandwich structures are explained. Literature findings reveal that dynamic and quasi-static compression behaviors of honeycomb sandwich structures are different. In accordance with the thesis objective, quasi-static and dynamic compressive behaviors were investigated separately in experimental studies. The data obtained from the dynamic and quasi-static compression tests were used for the validation study of the numerical models.

The Shimadzu AG-X universal testing machine used for tensile tests was used again with proper apparatus for quasi-static compression tests of honeycomb sandwich specimens. In this test setup, a stationary bottom plate was used as a base. Compression movement is provided by the top plate moving downwards at a constant speed.

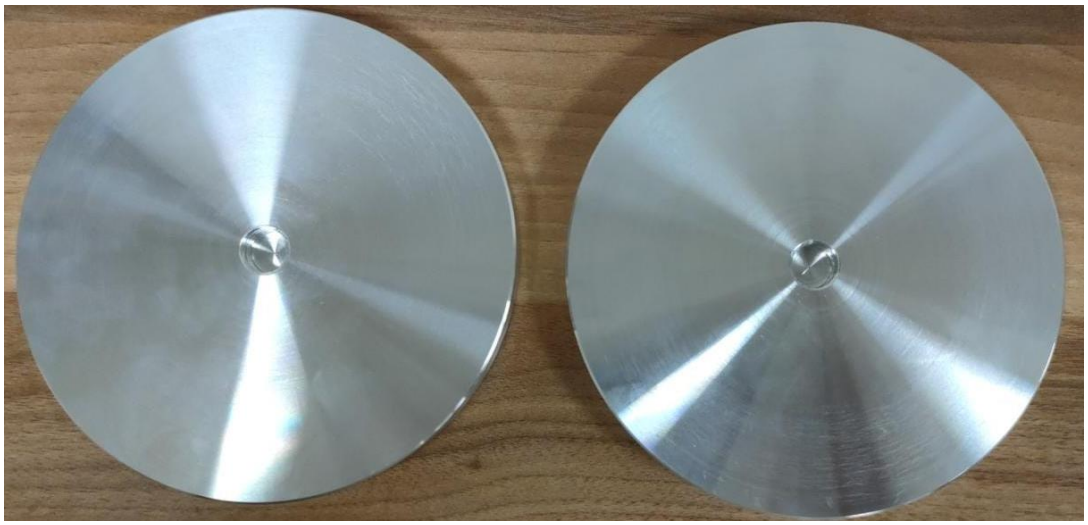

Figure 2.5. Top and bottom compression test plates of Shimadzu AG-X universal testing machine.

The target strain rate was generated by calculating the top plate velocity using the equation 2.1. During the compression test, a quasi-static strain rate of 10^{-3} s^{-1} was applied.

In the compression test, the compressive behavior of the honeycomb sandwich structure only in the through-thickness direction was investigated.

$$\dot{\varepsilon} = \frac{V}{L} \tag{2.1}$$

where ε is the strain rate; V is the cross-head velocity, L gauge length.

Figure 2.6. Fully crushed circular honeycomb specimen.

Markers are placed on the top and bottom plates for stroke measurement. The displacement between the markers was measured with a video extensometer. Video extensometer measurements were verified by comparison with stroke measurements obtained from the Shimadzu AG-X universal testing machine. Video capture was recorded until the end of the test to observe the folding mechanism of the honeycomb core.

2.2.2. Dynamic Tests

It is known that paper-based honeycomb structures exhibit different mechanical properties under dynamic loadings than they do under static loadings. So, in addition to static or quasi-static tests, dynamic tests are also necessary for the characterization of the dynamic mechanical behavior of paper-based honeycomb structures. Dynamic loading

conditions such as drop and topple are often encountered in the use of paper-based honeycomb sandwich packaging systems. Generally, strain rate ranges between 10^1 s^{-1} and 10^4 s^{-1} are accepted as dynamic loads. One of the most preferred testing methods for investigating the dynamic mechanical properties of materials at strain rates from 10^2 s^{-1} to 10^4 s^{-1} is the Direct Impact Test (DIT) setup. Since Direct Impact Testing is a custom test setup, there are some limitations and assumptions to collect accurate test results. Therefore, tests of low-strength materials such as paper-based honeycomb sandwich structures at high strain rates should be performed very carefully.

2.2.2.1. Dynamic Compression Test of Paper Honeycomb Specimens

Direct Impact test setup used in dynamic compression tests of paper-based honeycomb sandwich specimens basically consists of aluminum long bars, gas gun, and data collecting system. The illustration of the Direct Impact Test setup is given in Figure 2.7.

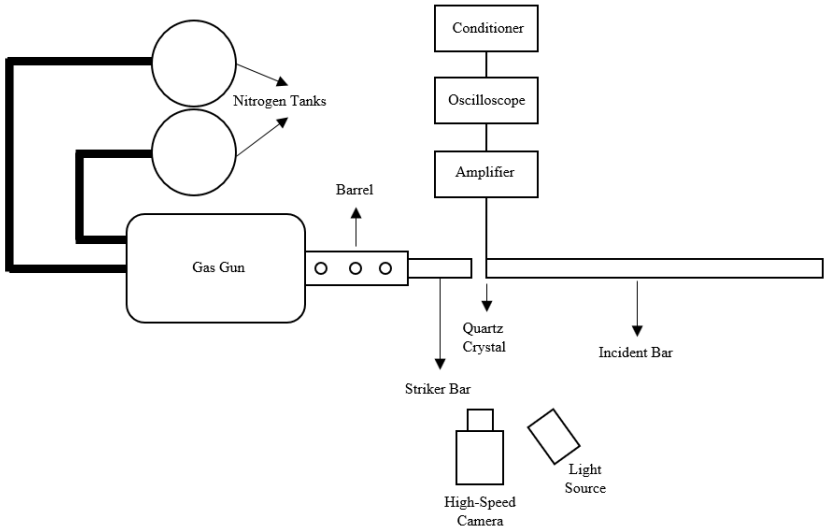

Figure 2.7. Illustration of Direct Impact test setup.

Bars of the direct impract test used in current setup consist of two cylindrical aluminum bars: striker bar (60 cm length), incident bar (199 cm length). All bars in the test setup are made of aluminum 7075-T6 with a diameter of 40 mm. In the test system, the rods are perfectly aligned, allowing them to move freely on their supports. Alignment

must be done carefully to minimize the effect of friction. The mechanical properties of the bar material Al 7075-T6 are given in Table 2.1.

Table 2.1 Properties of the material of bars (7075-T6 aluminum) [36].

Physical Properties	***Values***
Density	2810 kg/m^3
Elastic Modulus	71.7 GPa
Poisson's Ratio	0.3

For storing the compressed nitrogen gas, there are two nitrogen tubes. Nitrogen gas is sent through the pipes. One of the pipes fills the locking mechanism, while the other fills the loading mechanism. When the desired pressure value is reached, the valve is opened, and the gas gun is triggered. After triggering, the striker bar slide through a barrel attached to the gas gun. The velocity of striker bar is recorded with a two-point laser optical measuring device placed in the holes on the barrel. Thus, the speed provided by the compressed nitrogen gas to the gas gun is controlled as well.

Figure 2.8. DIT setup in Dynamic Testing and Modelling Laboratory

Piezoelectric quartz crystals were used to measure the force profiles at the interface where the specimen comes into contact with the bar. In the literature, It was stated that strain gauges are significantly less sensitive than quartz piezoelectric crystal

force transducers [31]. Paper-based honeycomb sandwich structures are materials that undergo high deformation at low stress values. For this reason, the use of piezoelectric crystals instead of strain gauges in dynamic characterization tests allowed more precise results to be obtained. Conductive epoxy was used to bond a piezoelectric quartz crystal between an aluminum disc and the tip of the incident bar. A quartz piezoelectric crystal electrical signal was obtained using a charge amplifier (Kistler 5010A), and this signal was then converted to a voltage value. Generated signals are monitored by an oscilloscope. Quartz piezoelectric crystal location between the bar-specimen contact region is shown in Figure 2.8.

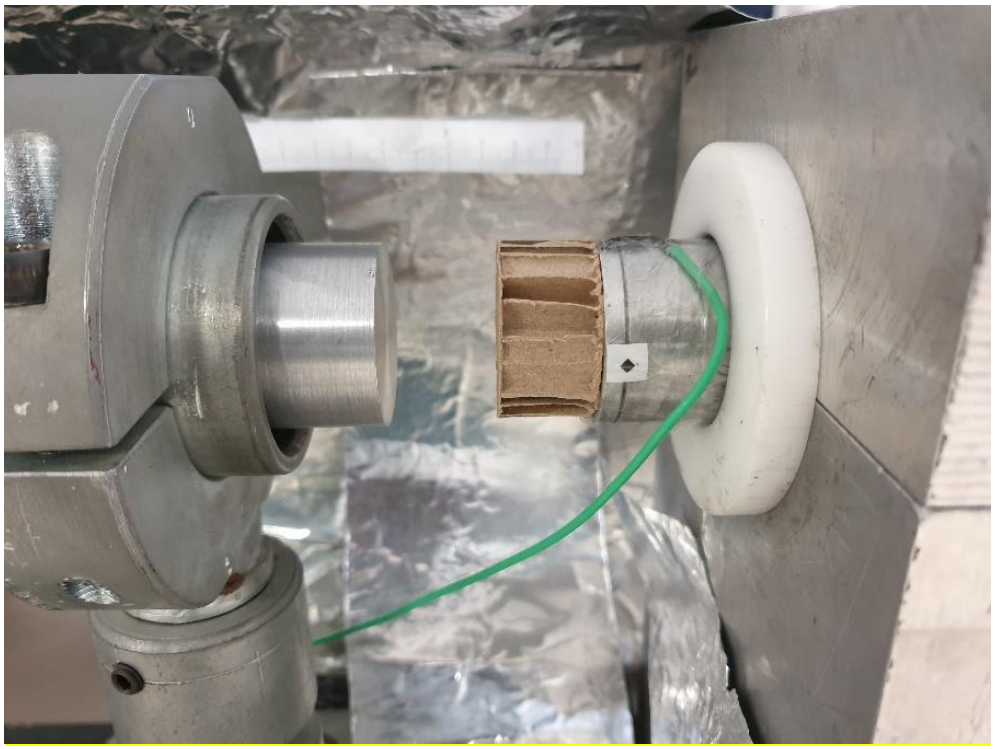

Figure 2.9. Piezoelectric quartz piezoelectric crystal location and circular test specimen.

In the Direct Impact tests, the compression behavior of the test specimen was recorded with the help of high-speed camera and a light source. Photron Fastcam SA1.1 was used as a high-speed camera. This high-speed camera is able to record up to 675000 fps under adequate lighting conditions. Dedolight spotlight is used in the high-speed video capturing setup. In Figure 2.9., high-speed camera and data collecting system for piezoelectric quartz crystal are shown.

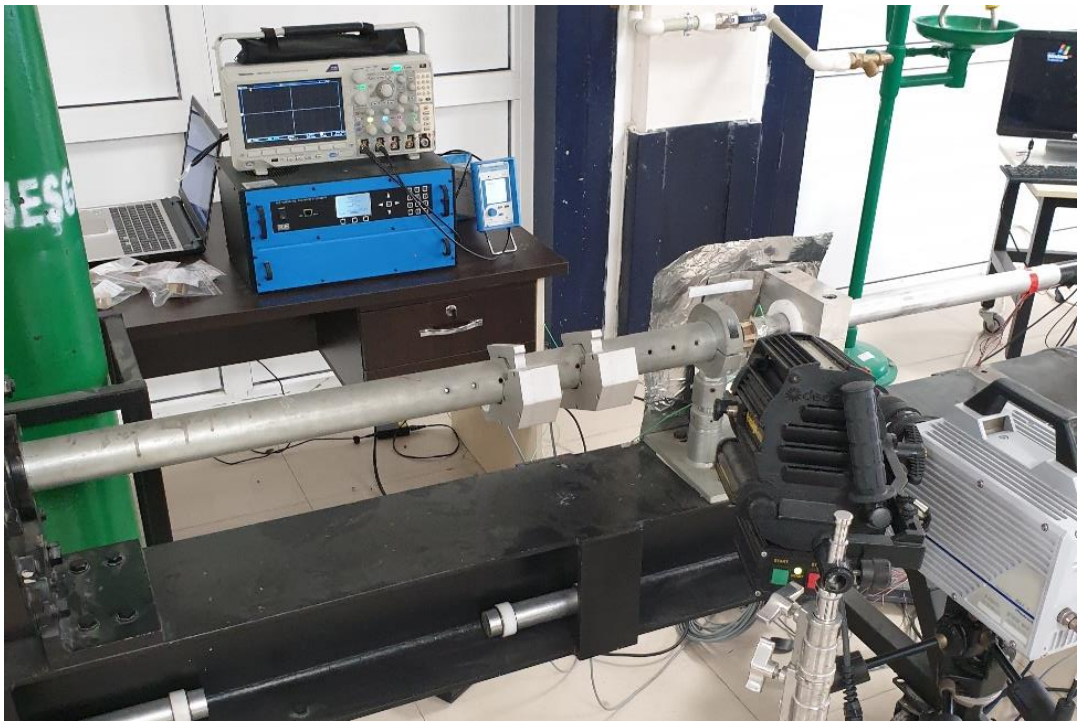

Figure 2.10. Data collecting system of Direct Impact test setup.

The direct impact test setup used in dynamic compression testing of paper-based honeycomb sandwich specimens was established in Dynamic Testing and Modeling Laboratory in IZTECH.

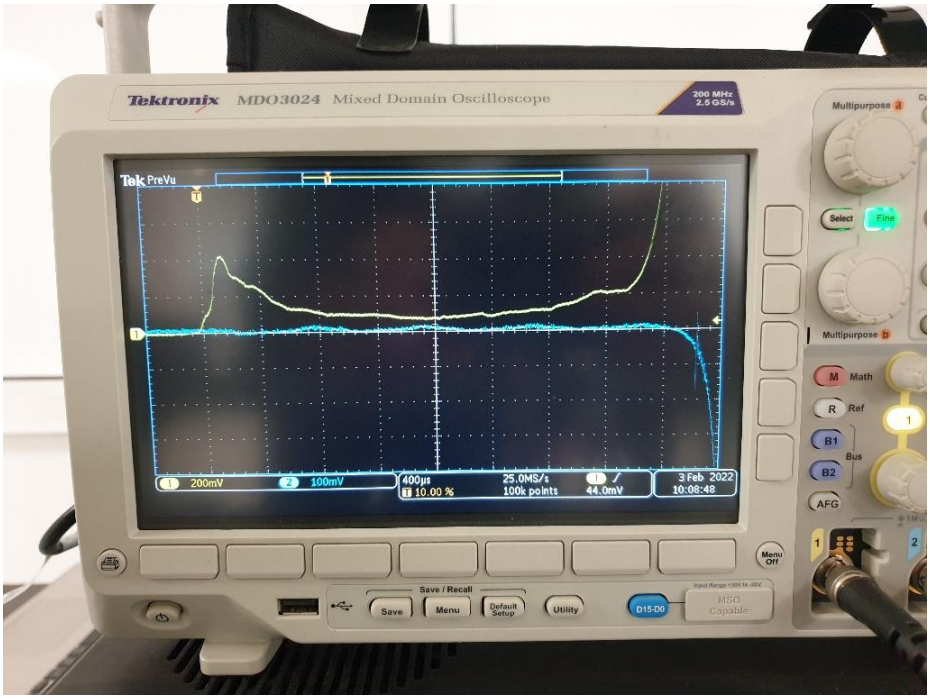

Figure 2.11. The dynamic response of honeycomb specimen on oscilloscope screen.

CHAPTER 3

NUMERICAL MODELING

The numerical modeling study of the paper-based sandwich specimen consists of CAD, mesh model creation, pre/post processing, and validation of numerical results with experimental results. After material characterization studies, numerical analyses were performed and a material card suitable to simulate the quasi-static and dynamic mechanical behavior of the kraftliner paper material was developed. A micro-mechanical modeling approach was preferred for the modeling of paper-based honeycomb sandwich structures. In this approach, the core walls and faces of the sandwich structure are modeled as 2D shell elements. With the help of the micro-mechanical modeling approach, the effect of energy absorption properties of core designs at the design stage can be examined without experimental tests. In addition, numerical modeling studies allow to examine the effect of micro-inertia, imperfections, strain rate sensitivity, and entrapped air in core cells. However, to obtain reliable numerical results, well-defined material inputs and boundary/initial conditions must be integrated into the FE tool in the proper format [38].

The finite element method (FEM) is a frequently used method for solving difficult engineering problems. Ls-Dyna is a commonly used finite element tool that deals with these complex physics, particularly in the automotive industry, aerospace, household appliance, and defense industries. This FE tool is especially utilized for explicit problems with multiple nonlinear problems. Nonlinearity is a result of unstable boundary conditions, high deformations, and material plasticity. In this study, the LS-Dyna FE tool was preferred because it offers multiple contact algorithms, suitable material model options, and arbitrary lagrangian-eulerian method.

In this section, the input parameters from the material characterization study, element formulation, and contact definitions are explained. The details about material card that can simulate material behavior at quasi-static and dynamic strain rates is also covered.

3.1. Material Model Development

Corrugated and honeycomb cardboard packaging systems made of this material are used in areas such as the packaging of household appliances and furniture. The main purpose of packaging systems is to protect the goods they contain in cases such as drop and topple. In the literature, it has been found that the mechanical properties of krafliner paper material and paper-based honeycomb structure change regarding strain rate values. Therefore, selecting a proper material card that includes the strain rate sensitivity effects is essential.

Being dependent on factors like strain rate, load type, temperature, relative humidity, and others makes the kraftliner material complex. The material shows nonlinear behavior, so it must be modeled using an appropriate material card that takes plasticity into account. Appropriate material models were investigated to accurately transfer the kraftliner material behavior observed in mechanical tests to numerical models. As a result of the research, it has been seen that the material models *MAT_24 PIECEWISE LINEAR PLASTICITY, *MAT_40 NONLINEAR ORTHOTROPIC, and *MAT_274 PAPER in the LS-Dyna material model library are frequently used in the modeling of paper and paper-like materials. In this study, *MAT_24 material model was used because it is suitable for the material input parameters obtained from the characterization studies and its efficiency in terms of modeling cost is high.

Kraftliner paper material has a fibrous structure due to its nature. For this reason, the material exhibits anisotropic behavior. The anisotropic behavior of the material is neglected in the use of the *MAT_24 material model. When the fiber alignment in the through-thickness direction of the honeycomb cores was examined, it was observed that the fibers in the core walls were oriented in the CD direction. For this reason, the data obtained from the quasi-static tensile test performed for the CD direction were used as the input parameters in the *MAT_24 material model.

In *MAT_24 material card, strain rate may be introduced with the Cowper and Symonds model. It defines the hardening by scaling the yield stress with a factor dependent on the strain rate value.

$$1 + \left(\frac{\dot{\varepsilon}}{C}\right)^{1/p} \tag{3.1}$$

Where $\dot{\varepsilon}$ is the strain rate, C and p are the Cowper and Symonds model constants.

Dynamic tensile test data were obtained from the literature [30] for a kraftliner paper that is very close to the specimens used in this study in terms of density and paper quality. After processing the obtained data, C and p parameters suitable for use in *MAT_24 model were obtained.

There are three different methods to define the plastic region in the *MAT_24 material model. The first of these is to define a feeding curve. The second option is to create a table containing the plastic zone values. The final option is to select eight data points from the plastic region and use them. In this study, the last option was chosen, and eight effective plastic strain values versus eight corresponding yield stress values were used to define the plastic region.

The specimens prepared for the quasi-static tensile test were weighed with the help of precision scales and the mass information was obtained. By calculating the specimen volume, the necessary density input for the material model was obtained.

Schulgasser [40] and Szewczyk [41] reported poisson's ratio values for various paper types between 0.2 and 0.375. The average value of 0.3 was used in the material model.

Table 3.1. MAT_24 material card inputs for CD direction properties.

ρ (kg/m^3)	E (MPa)	ν	σ_y (MPa)	C	p
808	556.8	0.3	7.07	387.92	5.42

The values given in Table 3.1 are used for the numerical modeling of all structural components in the sandwich structure.

3.2. Numerical Modeling of Experimental Tests

Two different solvers offered by Ls-Dyna were used in the numerical modeling of the mechanical tests. The first of these is the implicit solver used for quasi-static test models. The second is the explicit solver used for dynamic test models. In this section, mesh operation, contact algorithms, modeling of air, and other assumptions used in numerical models are explained.

3.2.1. Micro-Mechanical Modeling Approach

Experimental methods have physical limitations and sample or prototype preparation is not always cost-effective. To further investigation the effect of strain rate sensitivity, micro-inertia, and entrapped air on the compressive behavior of paper-based honeycomb structure, a micro-mechanical numerical modelling approach was developed.

By using a numerical modelling tool, it was possible to investigate the entrapped air and structural response mechanisms for any defined material and geometric parameter, thus providing a much more detailed observation of the dynamic response of the paper-based honeycomb structure.

Honeycomb specimens were designed in the CAD tool SpaceClaim and exported to the HyperMesh in supported file format. The 2D shell core wall and face geometries were discretized to quad (shell) elements in HyperMesh [42,43]. The numerical models of top plate, bottom plate, striker bar, and incident bar were established in the Ls-PrePost meshing tool directly without using the external CAD and meshing tool. Regarding the experimental setup, initial and boundary conditions were assigned. Post-processing were completed with the obtained numerical analysis outputs. Then the numerical results were validated with the experimental results. A representation of the modeling steps is presented in Figure 3.1.

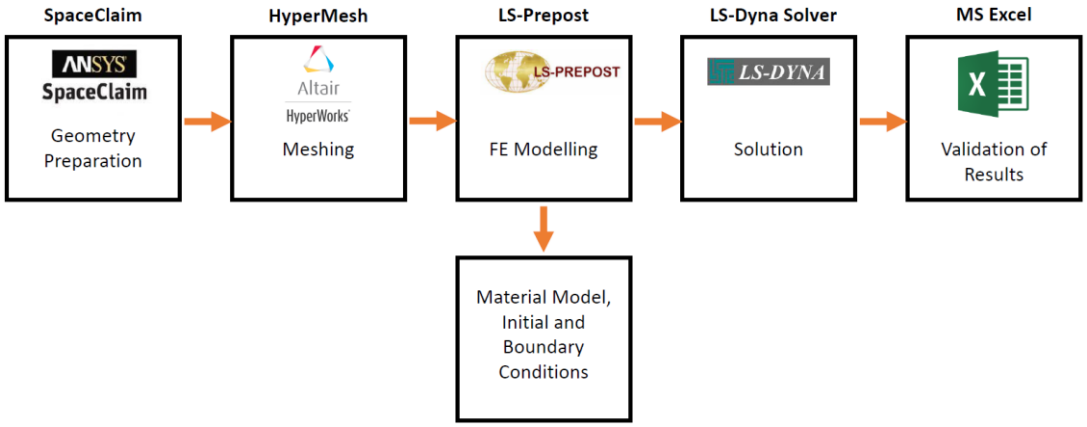

Figure 3.1. Representation of the modeling steps.

The top faces of the paper-based honeycomb specimens were peeled for core structure examination. According to the product datasheet provided by the supplier, the core diameter is 10 mm, and the core height is 20 mm. However, in the actual specimens, there are imperfections in the core structure. In order to increase the accuracy of the numerical results, instead of the core dimensions provided by the supplier, the imperfect core geometry was modeled in this study.

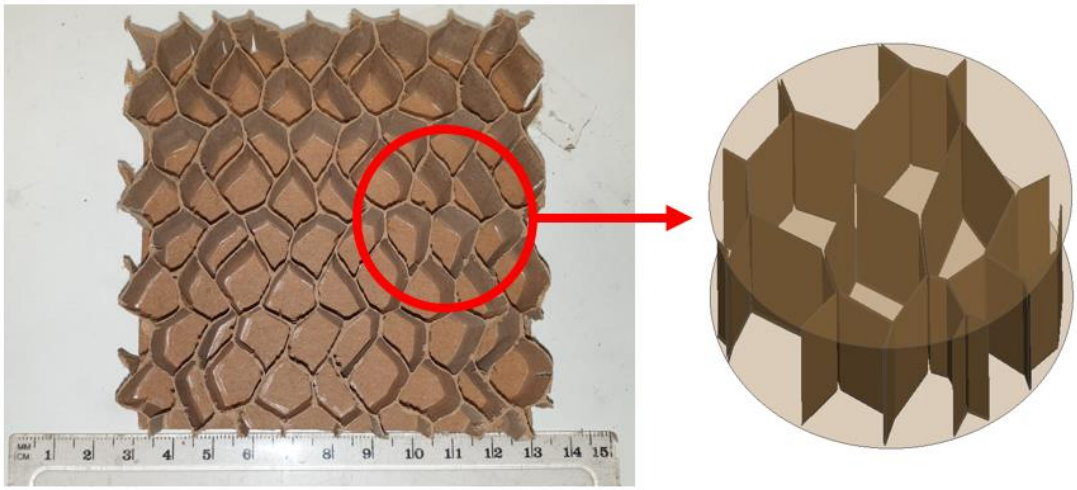

Figure 3.2. Specimen without top face and FE model

J.Reay [5] reported that element size directly affects the folding mechanism of the core in honeycomb sandwich structures. For this reason, 2D quad shell elements are used in 0.25 mm, 0.5 mm, and 1 mm sizes. It has been observed that the most efficient results in terms of computational cost and time among three different element sizes are obtained

when 2D quad shell elements with 0.5 mm size are used. Circular specimen geometry was discretized into 30640 four-noded 2D quad elements with six degrees of freedom per node. Shell element formulation ELFORM: 10 (Belytschko-Wong-Chiang) was selected. The shell integration point number is 4 in the thickness direction (default value is 2). It was found that this element formulation definition provided satisfying results at a reasonable computational time while maintaining numerical stability under large amounts of deformations.

A stiffness-based hourglass control type was developed in the study by Flanagan and Belytschko [32] to provide resistance to the undesirable hourglass forces and keeps their growth under control. This stiffness-based hourglass control type is available in the Ls-Dyna library. It has been observed that the Flanagan-Belytschko stiffness form provides the required numerical stability by keeping the hourglass energies to a minimum. Thus, it was defined for the shell parts of the honeycomb sandwich with *HOURGLASS keyword in dynamic compression test models. This value kept it as Ls-Dyna's default for the implicit solver.

Top plate, bottom plate, striker bar, and incident bar was modelled as linear-elastic material. Mechanical properties of Al 7075-T6 given in table 2.1. are used in the *MAT_001 ELASTIC material card.

Contact definitions allow FEM parts to touch, and prevent undesired initial penetrations, witout blocking the force transfer. Additionally, frictional effect between contact interfaces and to create permanent or temporary connection relationship between parts are simulated using contact definitions. LS-Dyna offers many contact types in its library. A detailed user guideline on this topic has been published by LSTC [39]. Suitable contact types were selected after reviewing the LSTC's user manual. Contacts must be assigned for every interface that is possible to touch, and must not penetrate each other, during the simulation. These definitions can be body to body, body to surface, body to body group, nodes to surface, depending on the model requirements. During the crushing of the honeycomb structure, contact definitions have been made for all parts that are expected to touch with each other. The thickness reaches 2t at the regions where the paper strips building the core structure bonded with each other. The adhesive is used to provide bonding in these contact areas. *AUTOMATIC ONE WAY SURFACE TO SURFACE TIE-BREAK contact type was assigned in these regions to include the adhesive effect in numerical models. This contact type automatically becomes inactive when it reaches the threshold value set by the user. According to the data reported in the study of J. Reay [5],

the values that can be used for the adhesive are between 62.5 kPa and 6.6 MPa. In the present study, the threshold value was accepted as 6 MPa.

Contact types *CONTACT AUTOMATIC SURFACE TO SURFACE and *CONTACT AUTOMATIC SINGLE SURFACE were assigned for predicted contact couples in the structure. These contact types are known as Penalty-Based contacts. In this contact assignments, contact option SOFT=1 (Soft-Constraint-based approach) is activated to prevent contact instabilities. In this contact option, the contact stiffness is calculated with respect to the nodal masses and the global time step size as shown in Equation 3.2. [38].

$$k = SOFSCL\frac{m}{\Delta t^2} \tag{3.2}$$

Where m is the nodal masses and Δt is the global time step size. The viscous damping coefficient (VDC) value was set at 20% to prevent fluctuations in contact force outputs because of the difference between stiffness values of metal bodies and paper-based structures. *CONTACT AUTOMATIC SURFACE TO SURFACE contact type prevents the parts from penetrating each other, while *CONTACT AUTOMATIC SINGLE SURFACE contact prevents penetrations that may occur if the parts are folded on themselves.

*TIED SHELL EDGE TO SURFACE OFFSET contact is used to provide the connection between the lower and upper core edges and faces. To avoid numerical instabilities, the bottom and top core elements are defined as separate parts, as suggested by J.Reay [5]. In this way, it is prevented that the boundary elements operating simultaneously under both tied and tie break contact boundary conditions. When the test specimens were examined, it was observed that the core ends were not connected perpendicularly to the faces. Core edges are connected to the faces at an angle. Therefore, it is aligned with a 45-degree angle between the bottom and top nodes of the parts defined as edge elements. The alignment of the core edge elements is shown in Figure 3.3.

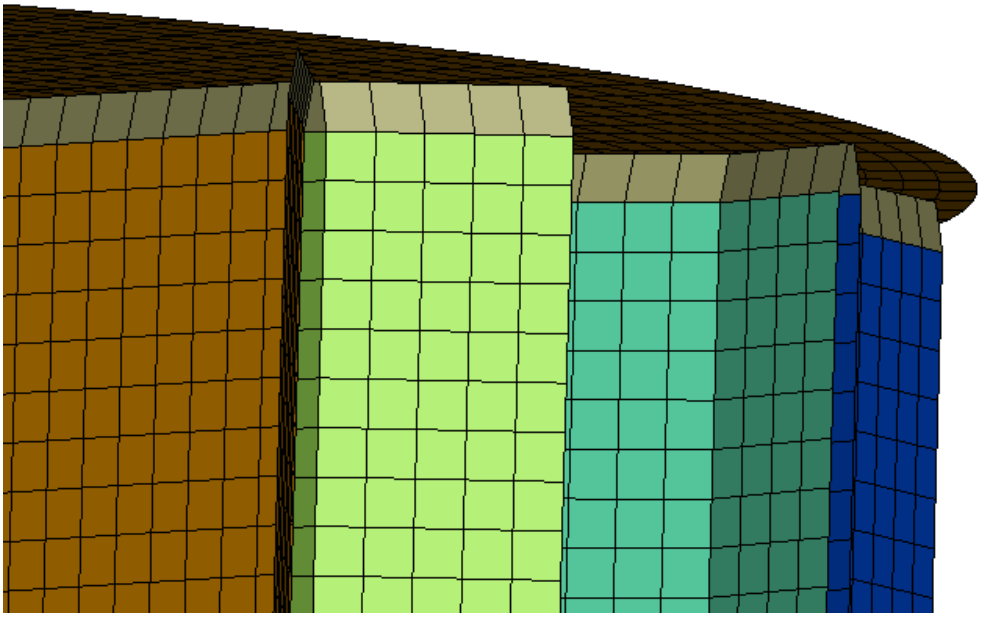

Figure 3.3. The alignment of the core edge elements.

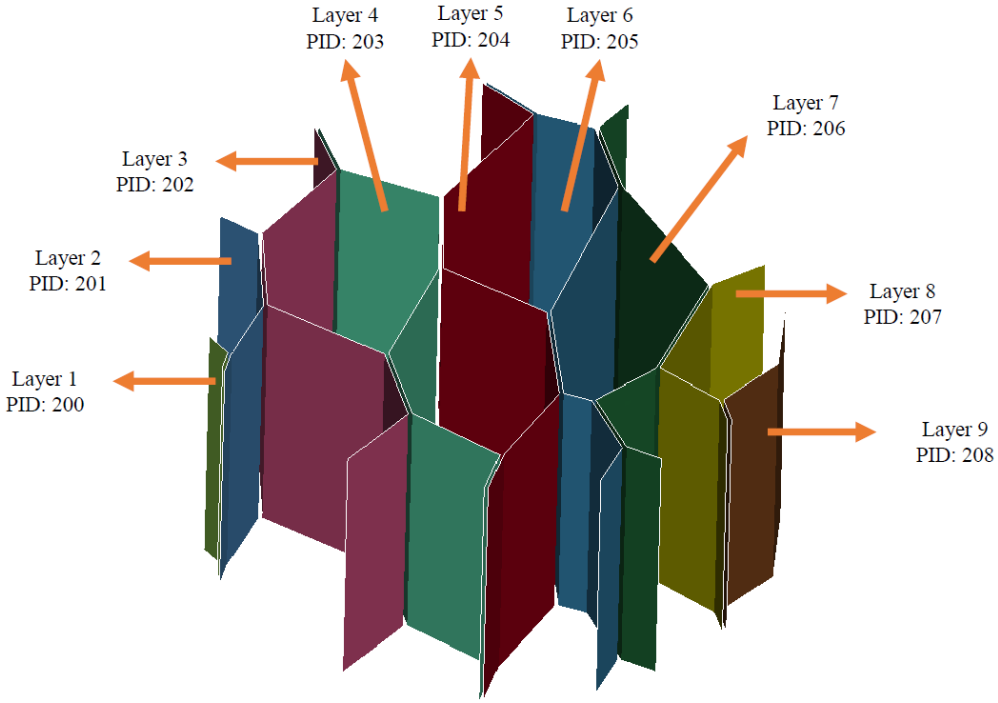

Figure 3.4. Part ID assignment of the core.

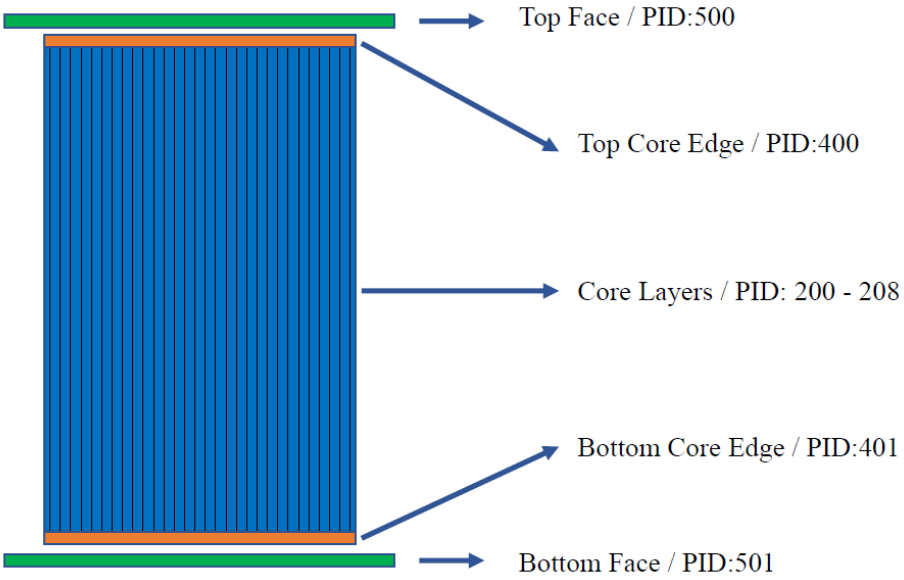

Figure 3.5. Main parts of numerical models.

Table 3.2. The contact assignments and part couples used in the numerical model of honeycomb sandwich structure, where C = Automatic surface to surface, Z = Automatic single surface, Y = Automatic one way surface to surface tie-break, D = Tied shell edge to surface offset.

PID	**200**	**201**	**202**	**203**	**204**	**205**	**206**	**207**	**208**	**400**	**401**	**500**	**501**
200	Z	C+Y	-	-	-	-	-	-	-	C	C	C	C
201	C+Y	Z	C+Y	-	-	-	-	-	-	C	C	C	C
202	-	C+Y	Z	C+Y	-	-	-	-	-	C	C	C	C
203	-	-	C+Y	Z	C+Y	-	-	-	-	C	C	C	C
204	-	-	-	C+Y	Z	C+Y	-	-	-	C	C	C	C
205	-	-	-	-	C+Y	Z	C+Y	-	-	C	C	C	C
206	-	-	-	-	-	C+Y	Z	C+Y		C	C	C	C
207	-	-	-	-	-	-	C+Y	Z	C+Y	C	C	C	C
208	-	-	-	-	-	-	-	C+Y	Z	C	C	C	C
400	C	C	C	C	C	C	C	C	C	-	C	C+D	C
401	C	C	C	C	C	C	C	C	C	C	-	C	C+D

When the quasi-static compression test results were examined, it was observed that the specimens passed into the densification stage when they were crushed about 18

mm. For this reason, in implicit models, it is ensured that the upper head moves 18mm in the -z-direction at 10^{-3} s^{-1} strain rate. The displacement curve was assigned using the *BOUNDARY PRESCRIBED MOTION SET card.

In the direct impact test, the strain rate value is approximately 317 s^{-1}. In order to obtain this strain rate value in numerical models, an initial velocity of 6.35 m/s was defined in the thickness direction by using the *INITIAL VELOCITY card. The masses of the striker and incident bars in the numerical models were adjusted in accordance with the direct impact test setup using the mass trimming tool in LS-Prepost.

In the literature, it has been found that the entrapped in the core cells affects the compressive behavior of the honeycomb structure [5,22,23]. For this reason, the entrapped air inside the core cells is modeled. The main objective of this modeling approach is to find the contribution rate of this effect on the compressive behavior of the structure by comparing the numerical results with and without entrapped air effect. The air packs inside the core cells whose structural integrity is intact were modeled using 3D solid brick elements. The volumes of the created air packs were adjusted to fill the cells completely.

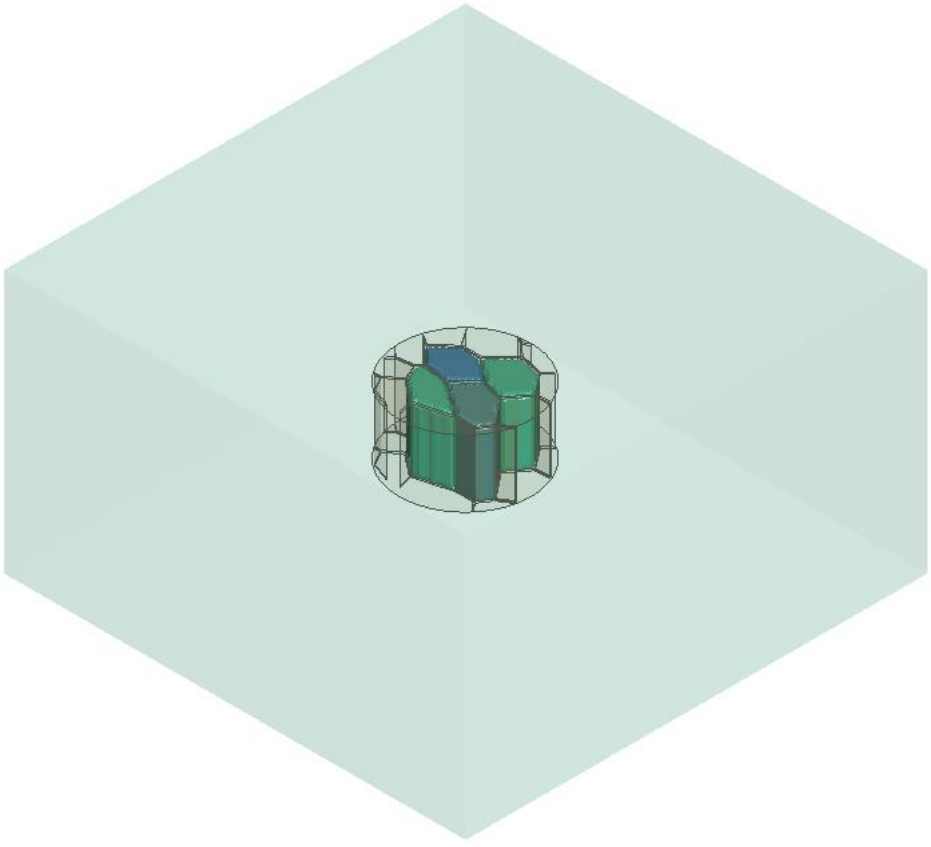

Figure 3.6. ALE background domain and air packs in core cells.

In Fluid Structure Interaction models Structured ALE method is used. S-ALE solver by LS-Dyna is an ALE solver that aims to solve ALE problems using structured mesh. It supports both parallel and serial solvers. It runs faster, uses less memory and is more stable than the classic ALE method.

Two keyword options are frequently preferred to define the pressure-volume relationship of air, *EOS LINEAR POLYNOMIAL and *EOS IDEAL GAS. Although both equations were examined, linear polynomial was used as the equation of state due to the higher numerical stability. *MAT NULL, a user-defined model, was used to model the air. In the analysis, the density of the air was assumed as 1.225 kg/m3. In order to observe the interaction of eulerian elements (fluids) with each other, each air pack and background domain were defined individually using the *ALE MULTI-MATERIAL GROUP card. These air packs, which are defined individually, are adjusted to completely fill the core cells with the help of the *INITIAL VOLUME FRACTION card. Contact of Eularian elements with structural parts is defined with *CONSTRAINED LAGRANGE IN SOLID card. With this definition, it is ensured that the compressed air applies pressure on the surfaces of cells during the crushing of the core structure. In addition, it also allowed the escape route of the entrapped air inside the core cells to the outside of the core structure to be observed.

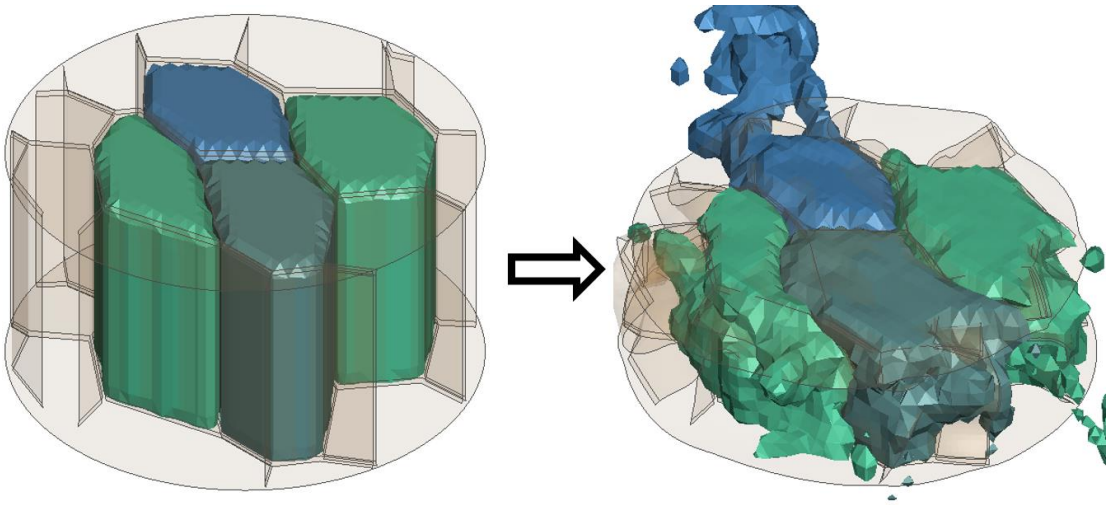

Figure 3.7. Fluid structure interaction

CHAPTER 4

RESULTS AND DISCUSSION

4.1. Kraftliner Paper Material Characterization Results

In the experimental studies, quasi-static tensile tests were carried out in accordance with ASTM D828-16 standard as mentioned in chapter 2. For tensile tests, four strip kraftliner specimens were prepared in MD and CD directions depending on the rolling direction of paper. Tensile load was applied to the specimens at 10^{-3} s^{-1} strain rate until the failure strain value was reached. During the test, force values were measured by the testing machine and strain values were measured by the video extensometer. The recording from tensile test is shown in Figure 4.1.

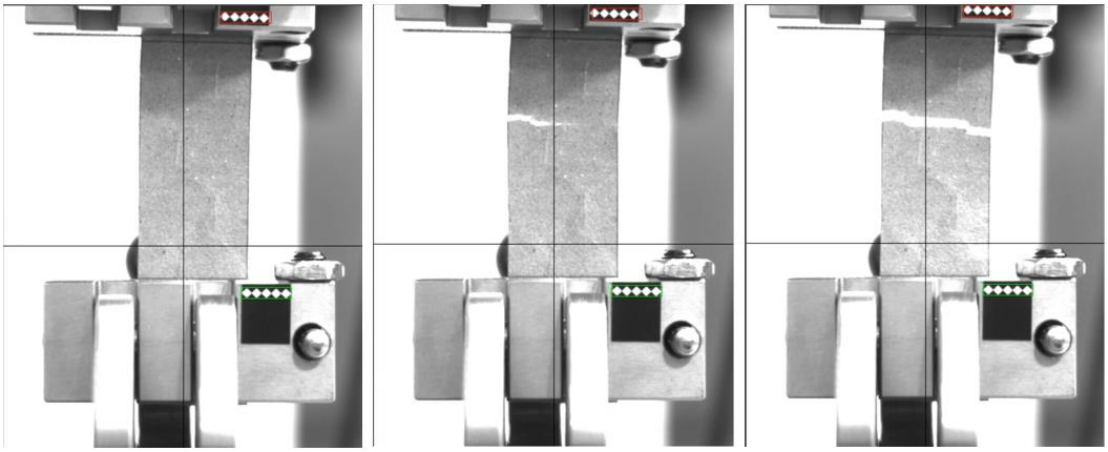

Figure 4.1. Video extensometer recording of tensile test.

The main purpose of performing the tensile test is to carry out the characterization study of the orthotropic paper material used as the cell wall and face. The result curves (Figure 4.2.) are similar to the curves shared in the study of Castro and Ostoja-Starzewski [28]. When the result curves are examined, the orthotropic behavior of kraftliner material is clearly observed.

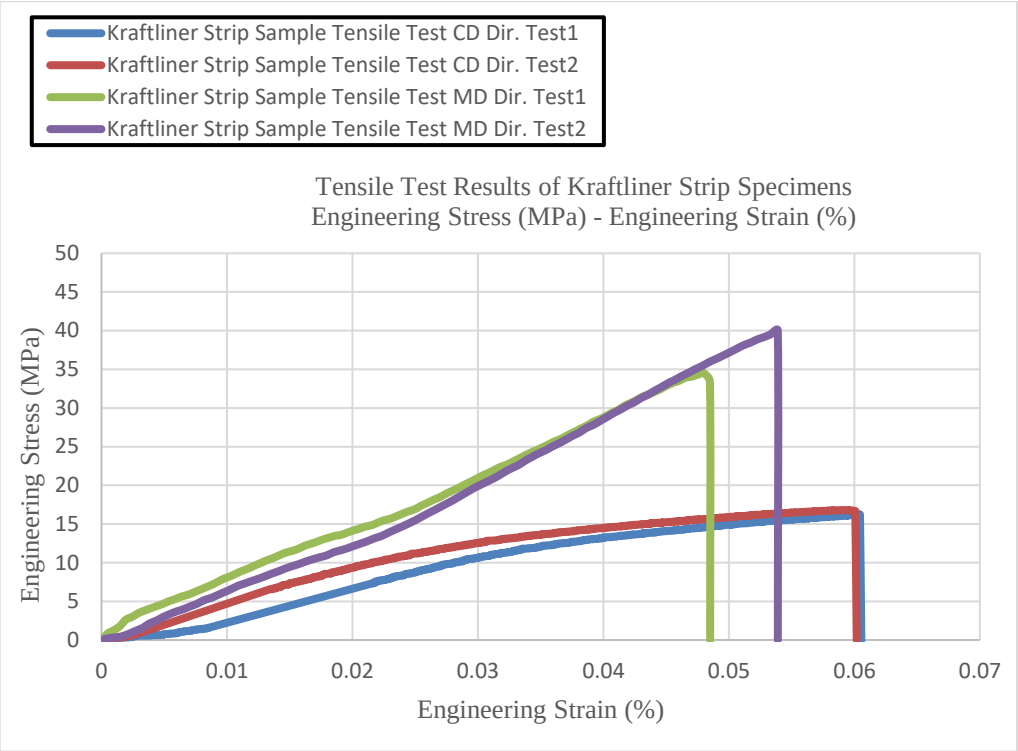

Figure 4.2. Tensile test results of kraftliner strip specimens

Scissor jaws were used to attach the specimens to the test equipment. A small amount of slipping of the paper strip specimens between the jaws caused fluctuations in the result curves. Although the use of adhesive was tried to prevent this sliding movement, it could not be applied because the adhesive would diffuse into the paper and affect the results.

Figure 4.3. Scissor jaws for tensile test.

Ultimate tensile strength (UTS) and failure strain (ε_f) values obtained from test curves are given in Table 4.1.

Table 4.1. Ultimate tensile strength (UTS) and failure strain (ε_f) values

Test Number	UTS (MPa)	ε_f (%)
Kraftliner MD Dir. Test 1	34.5	0.048
Kraftliner MD Dir. Test 2	40.02	0.054
Kraftliner CD Dir. Test 1	16.24	0.061
Kraftliner CD Dir. Test 2	16.79	0.06

Mechanical properties in CD direction were used in numerical modeling studies. The values used as input parameters in the LS-Dyna material card are given in Table 3.1.

4.2. Quasi-Static and Dynamic Compression Test Results

4.2.1. Quasi-Static Compression Test Results

In order to examine the quasi-static compressive behavior of paper-based honeycombs, six different tests were carried out with square and circular specimens. The dimensions shown in Figure 2.2. were used for square specimens, and the dimensions shown in Figure 2.3 were used for circular specimens. All specimens have the same core type. Quasi-static compression tests were carried out at 10^{-3} s^{-1} strain rate. During the quasi-static compression tests, force values were measured by the test device and strain values were measured by the video extensometer. Deformation images of square specimens taken from the video extensometer recording are given in Figure 4.4.

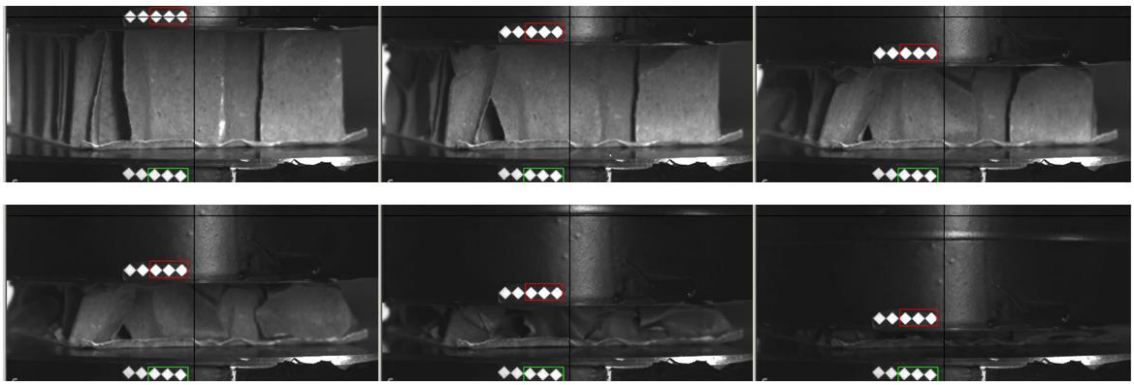

Figure 4.4. Video extensometer recording of square specimen quasi-static compression test.

The result curves obtained from the quasi-static compression test of square shaped paper-based honeycomb specimens are shown in Figure 4.5.

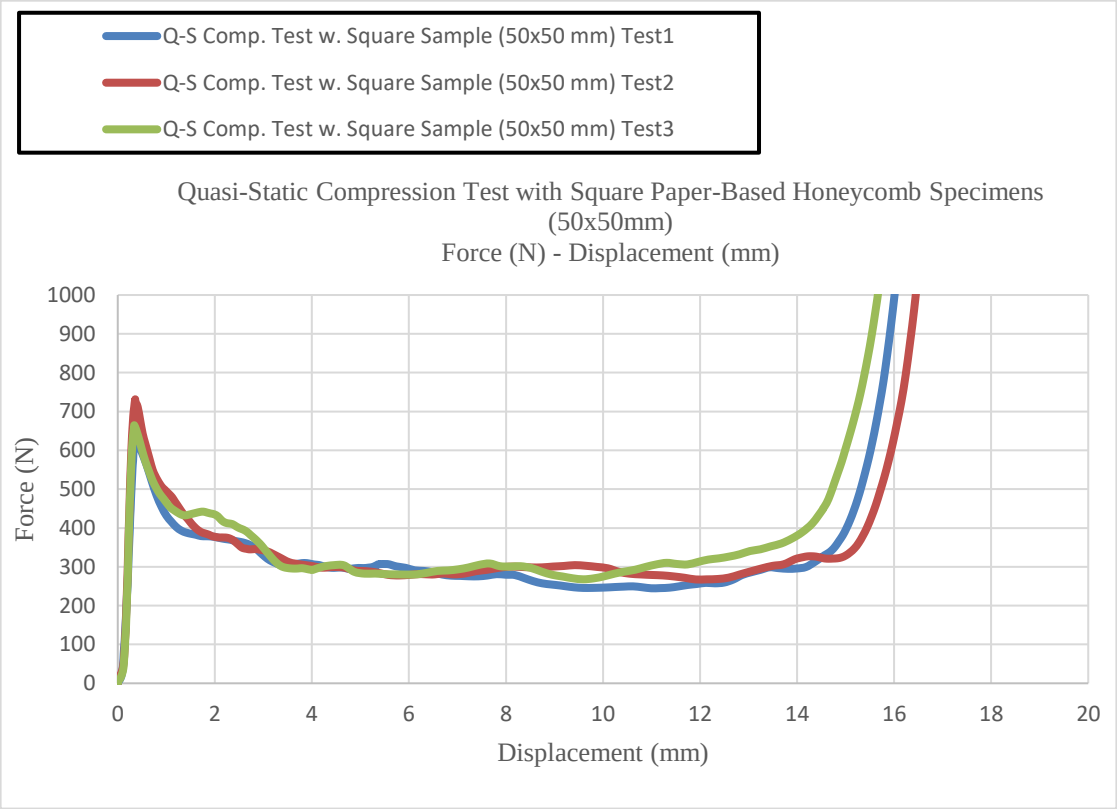

Figure 4.5. Force-Displacement curves of square specimen quasi-static compression tests.

The quasi-static compression test curves obtained for paper-based honeycombs showed typical honeycomb behavior under through-thickness compressive load, as expected. When the peak force values measured in three different tests performed with

square specimens were compared, it was observed that the peak force values were between 630.86 N and 731.47 N. In the plateau region, close force values were measured due to the similar folding behavior of the cell walls during the quasi-static compression tests. In the tests, it is seen that when the specimens reach roughly 75% strain value, cell walls complete the folding movement and the structure pass to the densification stage.

The direct impact test setup, which is used to investigate the dynamic compression behavior of paper-based honeycomb specimens, is a custom test setup. For this reason, the specimens to be examined in the direct impact test setup must have a circular cross-section with the same diameter as the striker bar. For this reason, circular specimens mentioned in Section 2.1 were prepared for dynamic tests.

In the studies from the literature, it has been stated that the total number of cells in the planform area of the specimens affects the compression behavior of the structure. Therefore, quasi-static compression tests were performed with circular specimens to make a reliable comparison with the dynamic test results.

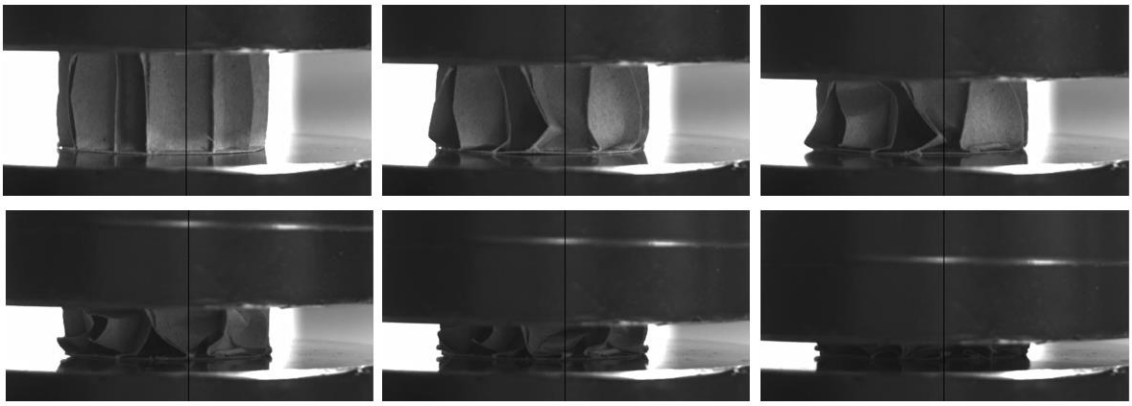

Figure 4.6. Video extensometer recording of square specimen quasi-static compression test.

The result curves obtained from the quasi-static compression test of circular paper-based honeycomb specimens are shown in figure 4.7.

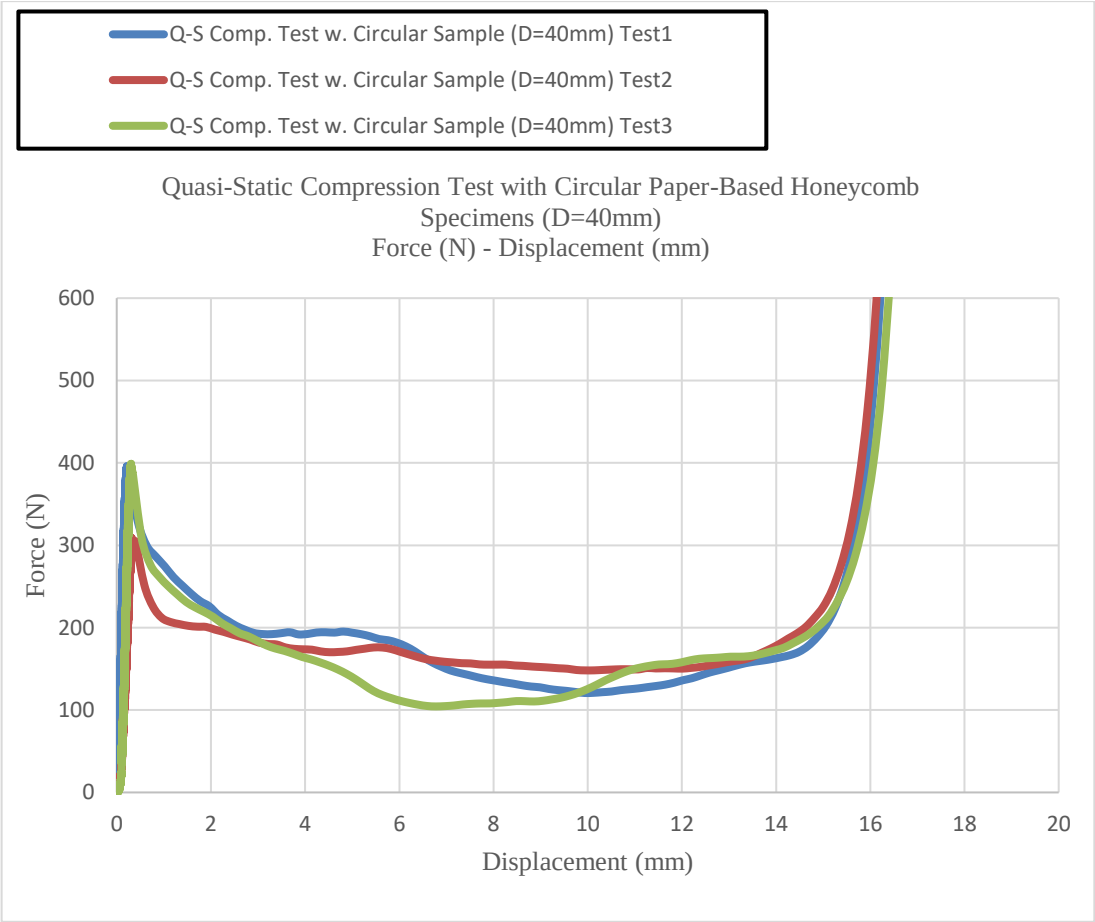

Figure 4.7. Force-Displacement curves of circular specimen quasi-static compression tests.

When the peak force values measured in three different tests performed with circular specimens were compared, it was observed that the peak force values were between 305.8 N and 396.3 N. In the plateau region, close force values were measured due to the similar folding behavior of the cell walls of the specimens during the quasi-static compression tests. In the tests, it is seen that when the specimens reach roughly 75% strain value, cell walls complete the folding movement and the structure pass to the densification stage.

The planform area, which is 2500 m^2 for square honeycomb specimens, decreases to 1256.6 m^2 for circular honeycomb specimens. For this reason, the number of complete cells in the planform area decreases. However, it is difficult to determine the exact number of complete cells in the core which is covered with faces. For this reason, the curves obtained for the square and circular specimens were compared by taking the average and the effect of the reduction in the planform area was investigated. The comparison curve is shown in Figure 4.8.

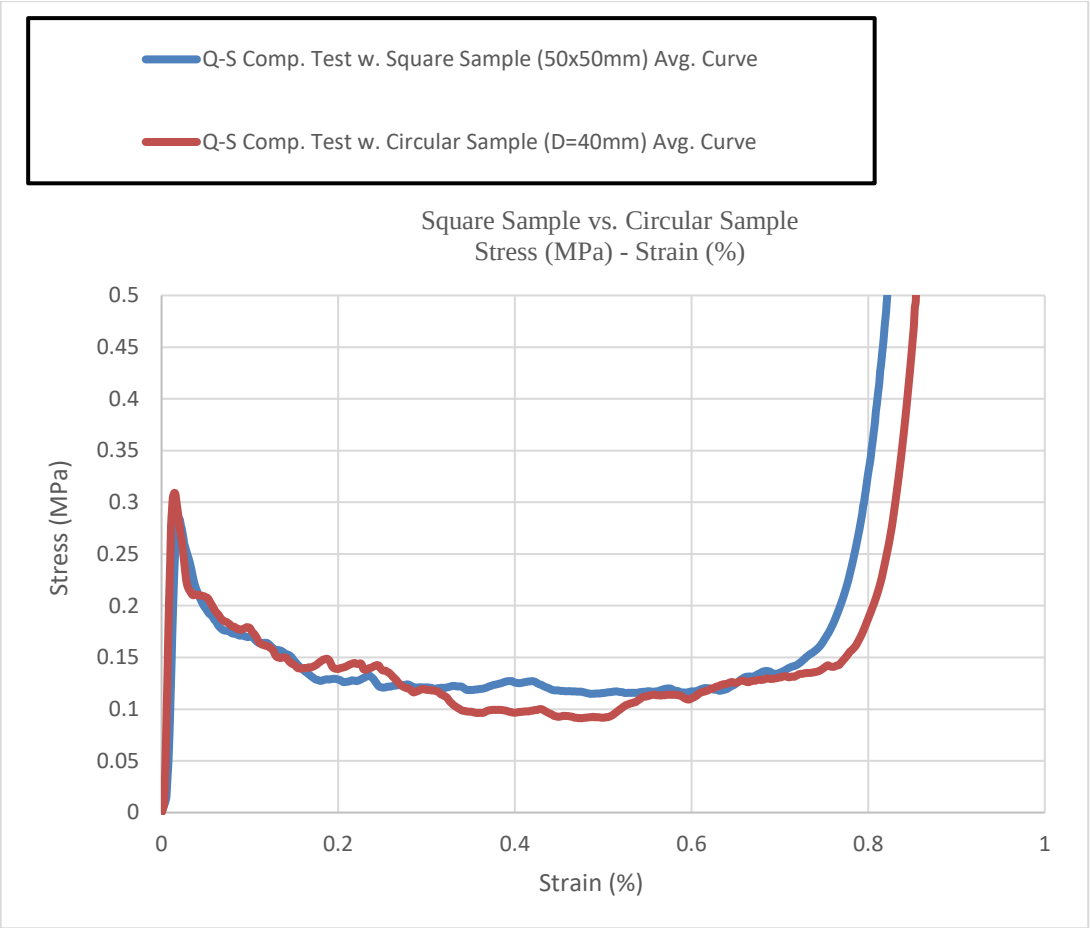

Figure 4.8. Comparison graph of quasi-static compression tests.

The average peak stress value for square specimens is 0.29 MPa. The average peak stress value is 0.31 MPa for circular specimens. A difference of about 0.02 MPa is observed between the two values. The decreasing stress values after the peak stress and the stress values in the plateau region are similar for both curves. However, in the average curve of the square specimens, it is observed that the square-shaped structure enters the densification stage a little earlier.

As a result, no significant differences were found between the compression behavior of the two specimen types. For this reason, it was decided to use the circular cross-section specimen geometry as a reference in numerical modeling studies.

4.2.1. Dynamic Compression Test Results

In order to examine the dynamic compressive behavior of paper-based honeycombs, two different tests were carried out with circular specimens. The

dimensions shown in Figure 2.3. for circular specimens. All specimens have the same core type. Dynamic compression tests were performed between 293 s^{-1} (5.86 m/s) and 317 s^{-1} (6.35 m/s) strain rates. During the dynamic compression tests, force values were measured by the data collecting system in the test setup and displacement values were measured from high-speed camera captures. Deformation images of circular specimens taken from the high-speed camera captures are given in Figure 4.9.

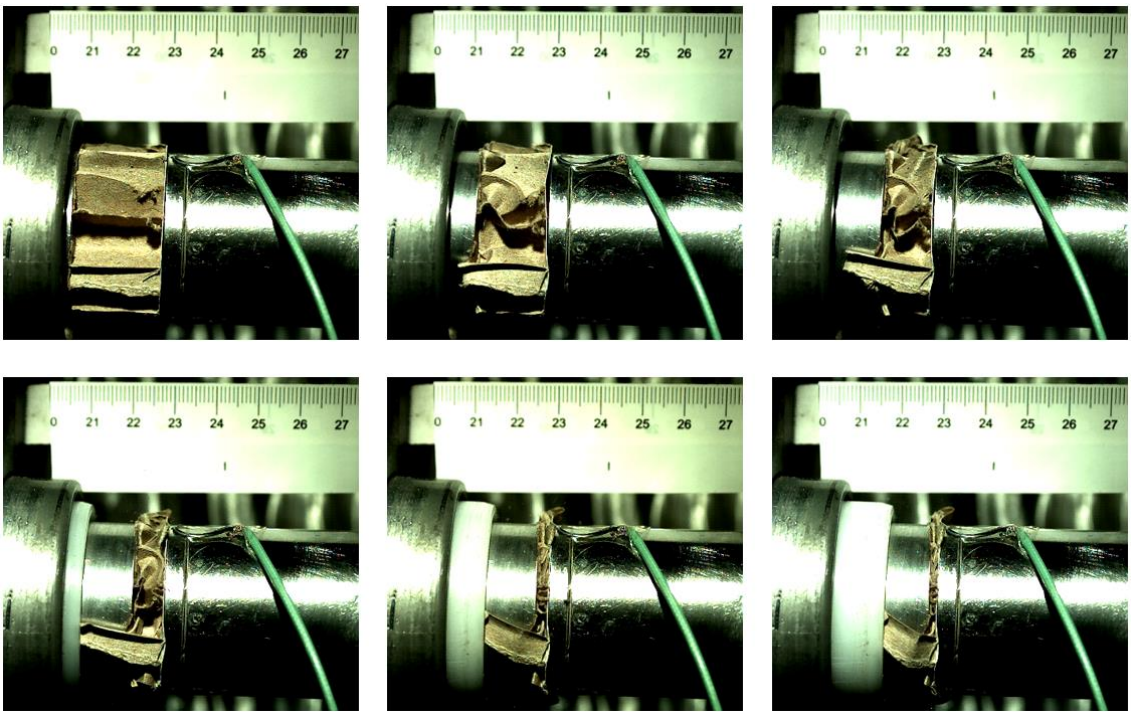

Figure 4.9. Direct impact test high-speed camera recordings.

The result curves obtained from the dynamic compression test of circular paper-based honeycomb specimens are shown in Figure 4.10.

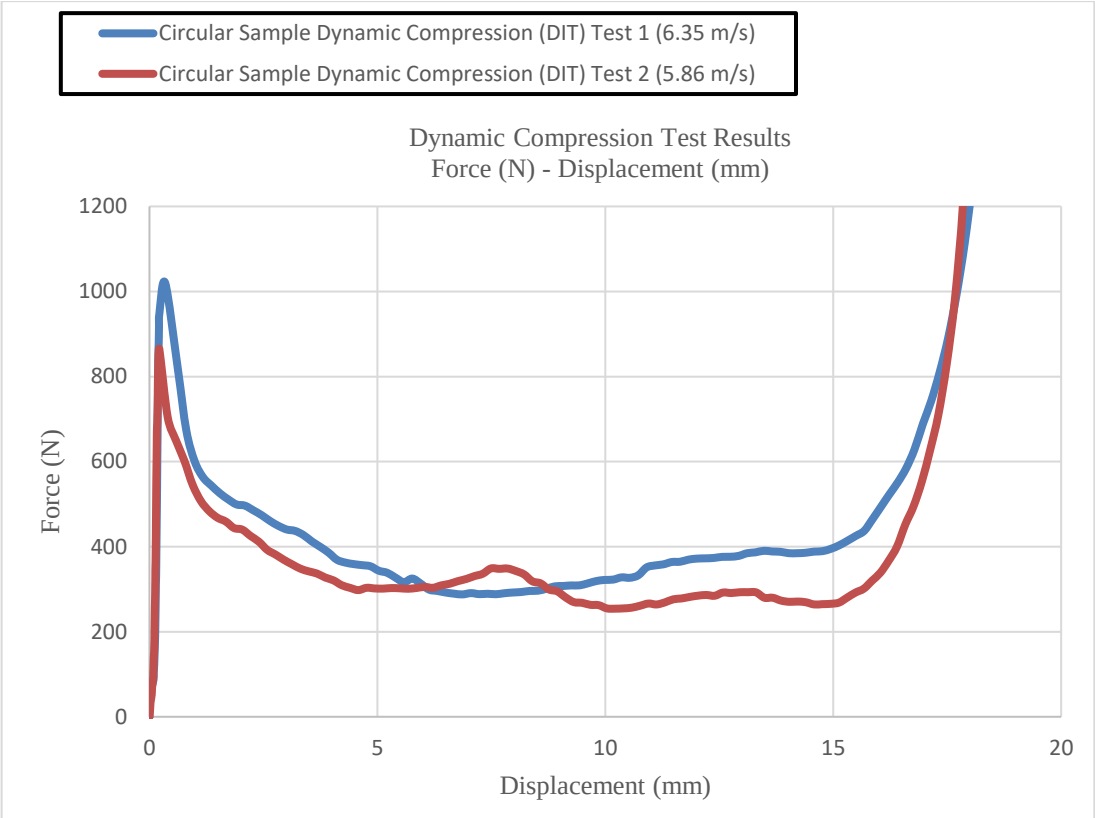

Figure 4.10. Force-Displacement curves of dynamic compression tests.

In dynamic compression test result curves, the peak force value for Test 1 is 1019.5 N. For Test 2, the peak force value is 864 N. A difference about 155.5 N is observed between the two values. The decreasing force values after the peak point and the force values in the plateau region are similar for both curves. Similar to the quasi-static tests, both specimens passed into the densification stage after crushing about 15 mm. However, a significant increase is observed in the measured force values compared to the quasi-static test values.

The quasi-static compression test curve and the dynamic compression test curve were compared to investigate the change in compressive behavior of paper-based honeycomb specimens due to increasing strain rate. In order to find the percentage difference between the two curves, the area under the curve between the displacement value corresponding to the peak force and the densification displacement value was calculated by integration. As a result of the calculation, it was calculated that the percentage increase between the quasi-static compression test and the dynamic compression test was 136.19%. This result reveals that there is a significant difference between the quasi-static and dynamic response of the structure.

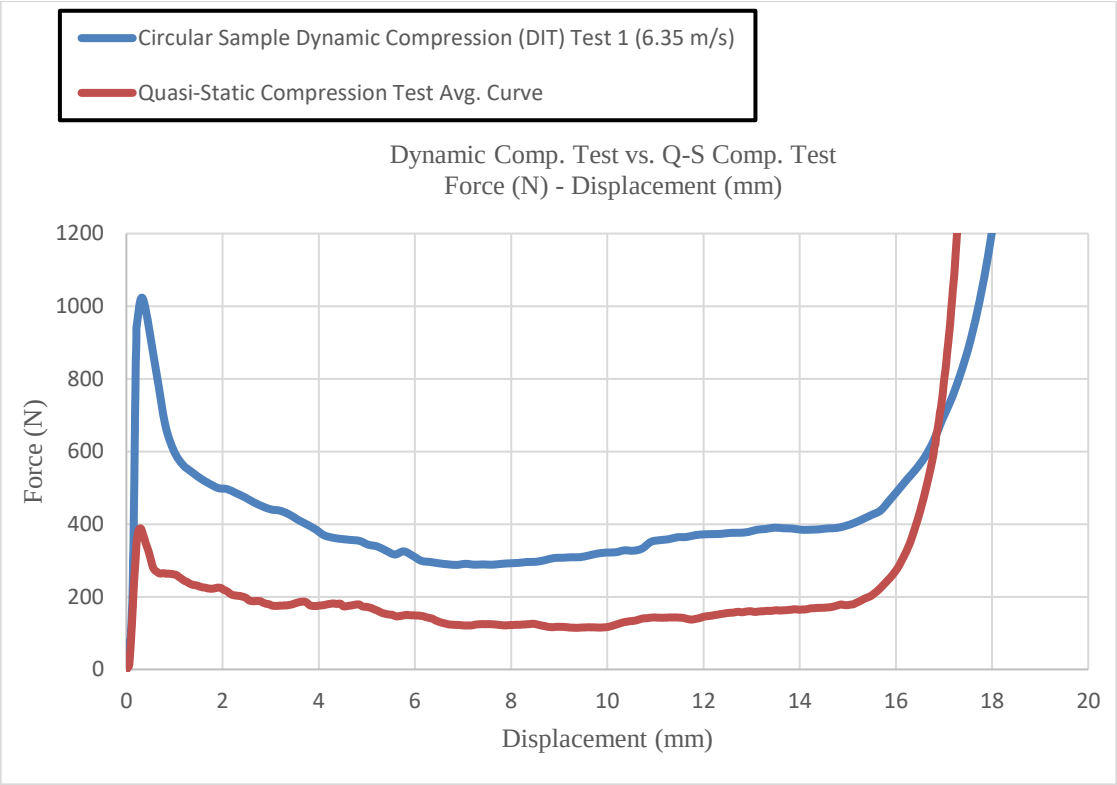

Figure 4.11. Comparison of dynamic and quasi-static compression test results.

4.3. Validation of Implicit and Explicit Numerical Models

In this section, the results of the experimental and the numerical results are compared and the accuracy of the numerical models was verified. In the comparison curves, dynamic compression test curve was used for the validation of the explicit model, and quasi-static compression test curve was used for the validation of the implicit model. The difference between the experimental and numerical results was calculated by comparing the peak force values and the areas under the curves. In addition, the percentage force increase-displacement curve was created, and the force increase percentages calculated separately in different regions of the force-displacement curve. In this way, it was investigated in which region the effects played a more dominant role.

Firstly, the numerical model including strain sensitivity of paper layer material and entrapped air effect was compared with the dynamic compression test result. Comparison of dynamic compression test and explicit model results is given in the Figure 4.12.

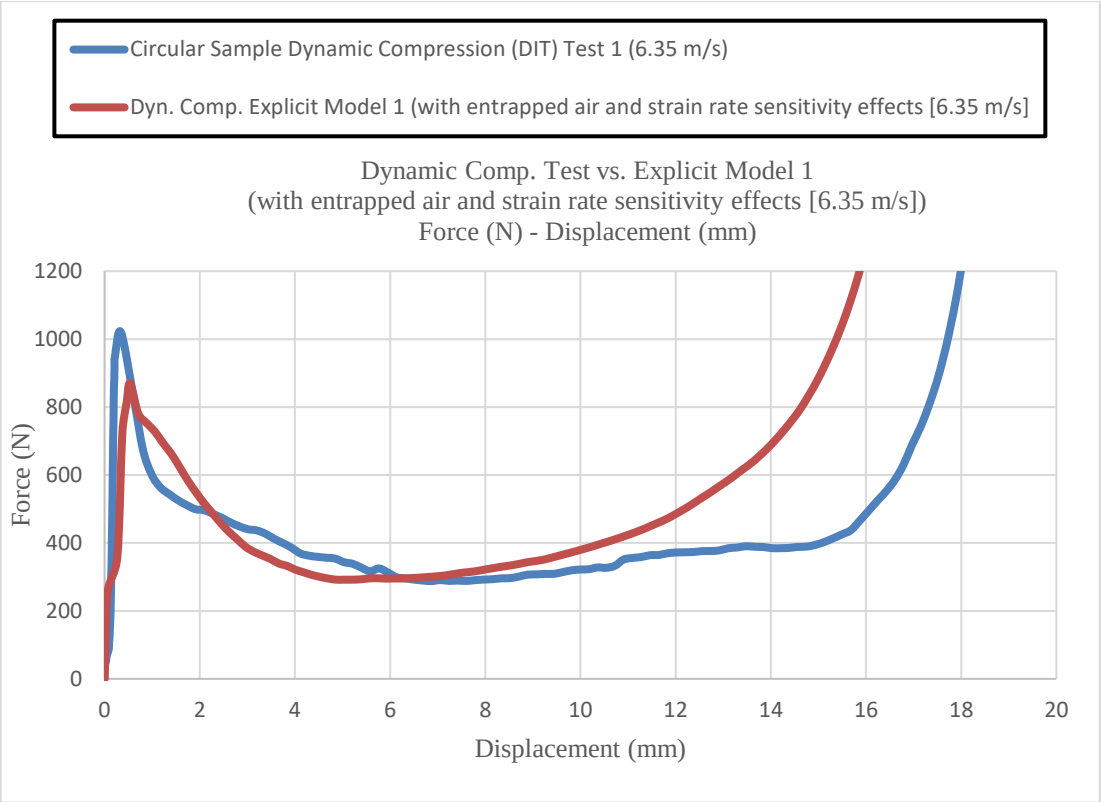

Figure 4.12. Comparison of dynamic test and explicit model 1 (with entrapped air and strain senstivity effects) results.

The peak force values of dynamic compression tests for paper-based specimens range from 864 N to 1019.5 N. The peak force value measured as 870.13 N in the explicit numerical model. Numerical peak value is in this range. However, in dynamic compression tests, unlike numerical models, a rapid decrease is observed in the measured force values after the peak force. The force values measured for the plateau region in the numerical model have good correlation with the tests. A significant difference is observed between the numerical and experimental results in the transition values of the densification region. The main reason is that the core-face connections of the specimens can be separated or peeled during deformation, but the connection cannot be separated due to the TIED contact type, which provides a permanent contact between core-face connection in numerical models. This situation causes an additional constraint and leads to an increase in force values by locking the folding mechanism after 50% strain.

After curve integration, the percentage difference between dynamic test and explicit model curves was observed to be 8.67%.

After the validation study was completed for the explicit model, the same process was repeated for the implicit model. The force-displacement curve obtained from the

quasi-static compression test was used for the validation of the implicit model. Since it is known that the effect of entrapped air has a significant effect at high strain rate loadings, it is not included in the implicit models. Comparison of quasi-static compression test and implicit model results is given in the Figure 4.13.

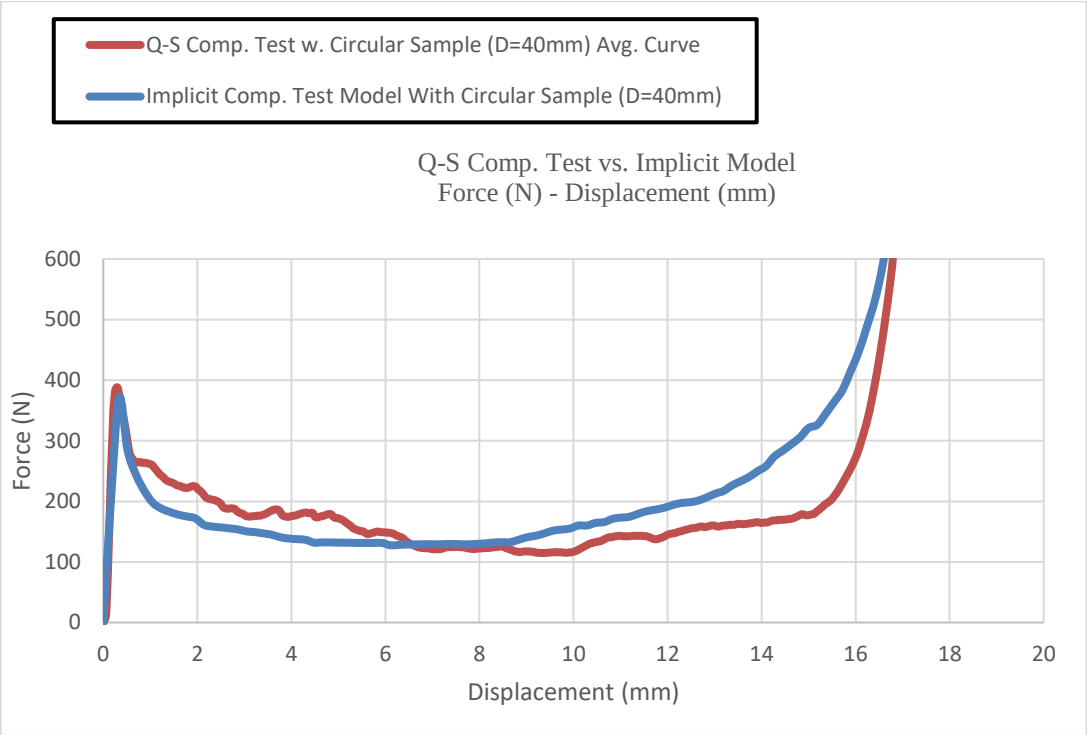

Figure 4.13. Comparison of quasi-static compression test and implicit model results.

The peak force value on the quasi-static compression test curve is 388.36 N. This value was measured as 371.4 N in the implicit model curve. Similar to the explicit model curve, an increase in force values was observed after 50% strain value in the implicit model. After curve integration, the percentage difference between quasi-static test and implicit model curves was observed as 4.15%.

4.4. Comparison of Numerical Models

Within the scope of this thesis, FE models of honeycomb specimens with the same geometric parameters were established. As mentioned in the previous sections, an implicit model was established to investigate the compressive behavior under quasi-static loads, and four explicit models were established to investigate the compressive behavior under

dynamic loads. By using FE tools, it is aimed to measure the effects of strain rate sensitivity, air trapped inside the cell and micro-inertia on the dynamic compressive behavior of the paper-based honeycomb structure. In this way, the contribution percentage of the effects which are difficult to measure in experimental studies, to the compressive behavior of the paper-based honeycomb structure were calculated by using FE tools.

When the dynamic and quasi-static compression test results were compared, it was observed that the difference between the curves was 136.19%. For this reason, explicit and implicit model results were compared using the same comparison method. As a result of the comparison, the difference between the model curves was calculated as 150.48%.

Comparison of explicit model and implicit model results is given in the Figure 4.14.

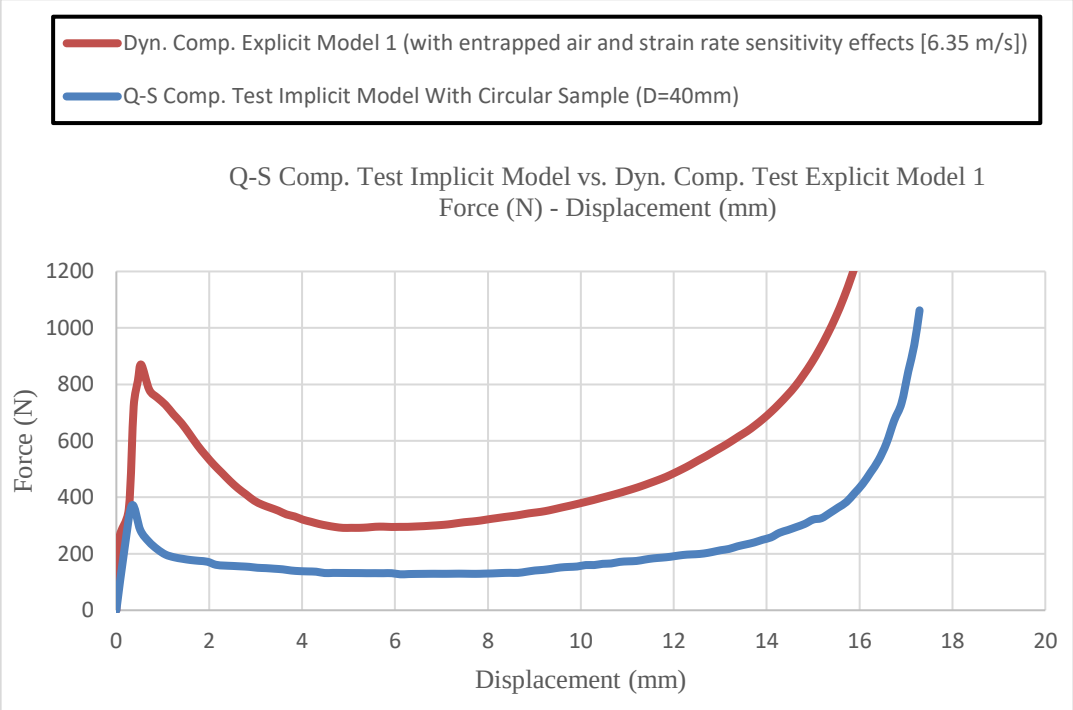

Figure 4.14. Comparison of explicit model 1 and implicit model results.

In order to examine the effects that change the dynamic compressive behavior, four different explicit model scenarios were prepared. Explicit model names and corresponding cases are shown in Table 4.2.

Table 4.2. Scheme of explicit models for dynamic compression test.

Model Name	Cowper-Symonds Parameters	Entrapped Air in Core Cells	Model Objective
Explicit Model 1	Included	Included	Actual Case
Explicit Model 2	Included	Excluded	Effect of Entrapped Air
Explicit Model 3	Excluded	Included	Effect of Strain Rate Sensitivity of Paper
Explicit Model 4	Excluded	Excluded	Effect of Micro-Inertia

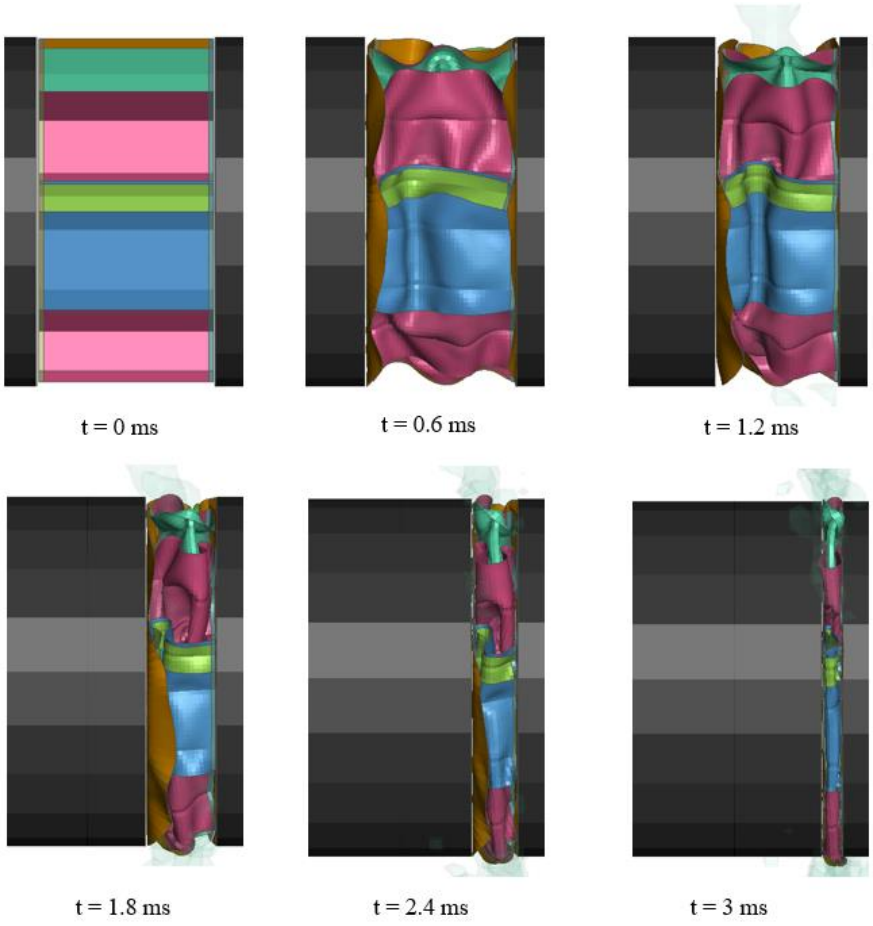

Figure 4.15. Deformation stages from explicit model.

In Figure 4.16., force - displacement curves obtained from Explicit Dynamic Compression Test Model 1 (with all effects) and Model 2 (without entrapped air effect) results are compared. In Explicit Model 2, the FEM definitions used to simulate the entrapped air are neglected. While the peak force was measured as 870.14 N in the model including the entrapped air effect (Model 1), the peak force value was measured as 860.2 N in the model in which this effect was neglected (Model 2). In order to find the percentage difference between the two curves, the area under the curve between the displacement value corresponding to the peak force and the densification displacement value was calculated by integration. After curve integration, the percentage difference between entrapped air effect included and excluded model curves was observed as 7.08%.

Figure 4.16. Comparison of explicit model 1 and explicit model 2 results.

The only variable that differs between models is the effect of entrapped air. Based on this result, the contribution percentage of the entrapped air inside the core cells on the dynamic compression behavior of the structure was evaluated as 7.08%.

Another effect that contributes to the dynamic response of the structure is strain rate sensitivity. Cowper-Symonds parameters are defined in the material card to introduce the strain rate sensitivity of the cell wall and face material in micro-mechanical models.

The defined parameters affect the strain-rate dependent hardening behavior of the cell wall and face material after the yield point, depending on the Cowper-Symonds equation. In Explicit Model 3, the Cowper-Symonds parameters in the material card have been removed. Thus, strain-rate sensitivity caused by the paper layer material was ignored. The comparison of the model results obtained by ignoring the strain rate sensitivity and Explicit Model 1 (with all effects) results are shown in Figure 4.17.

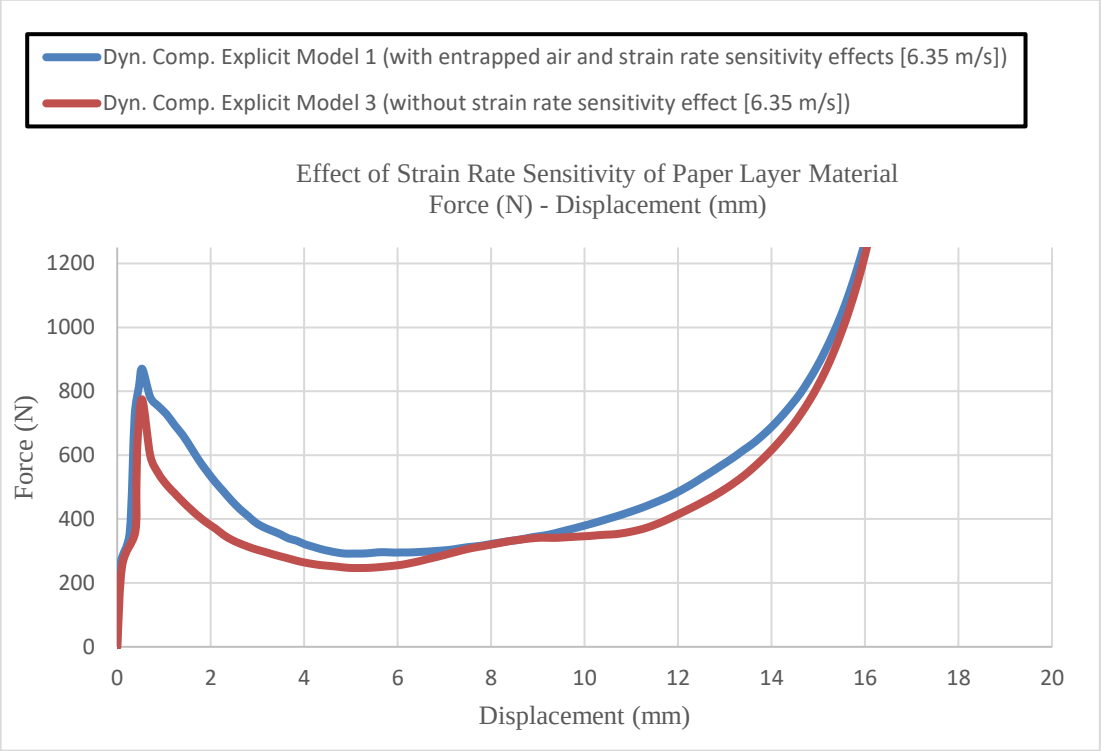

Figure 4.17. Comparison of explicit model 1 and explicit model 3 results.

As it can be seen from the force-displacement graph, ignoring the strain rate sensitivity parameters caused a decrease in strength values. While the peak force for Model 1 was 870.14 N, the peak force for Model 3 was 774.16 N. After curve integration, the percentage difference between Explicit Model 1 and Explicit Model 3 curves was observed as 18.02%. This difference observed between the two curves represents the contribution percentage of the strain rate sensitivity.

Finally, the effect of micro-inertia on dynamic compression behavior was investigated. Explicit Model 4, which ignores the strain rate sensitivity of the paper layer material and the effect of entrapped inside the core cells, was established to investigate the micro inertia effect. Comparison of Model 4 and Model 1 results is shown in Figure

4.18. While the peak force for Model 1 was 870.14 N, the peak force for Model 4 was 767.81N. After curve integration, the percentage difference between Explicit Model 1 and Explicit Model 4 curves was observed as 32.51%. The difference calculated between the two curves represents the force drop that would be observed when the combined effect of strain rate sensitivity and compressed air is neglected. The curve obtained from model 4 is compared with the implicit model result only to determine the contribution rate of the micro-inertia effect. As a result of the comparison, the difference between the two curves was calculated as 96.56%. This difference calculated between the two curves represents only the micro-inertia induced force increase. It should be noted that when the entrapped air effect is included in the models, the air bursts the double-thickness walls as it escapes. The separation of double-thickness walls may affect the contribution rate of the micro-inertia effect. For this reason, the micro-inertia effect to be observed in the entrapped air effect included models may change depending on the deformation that will occur in the structure.

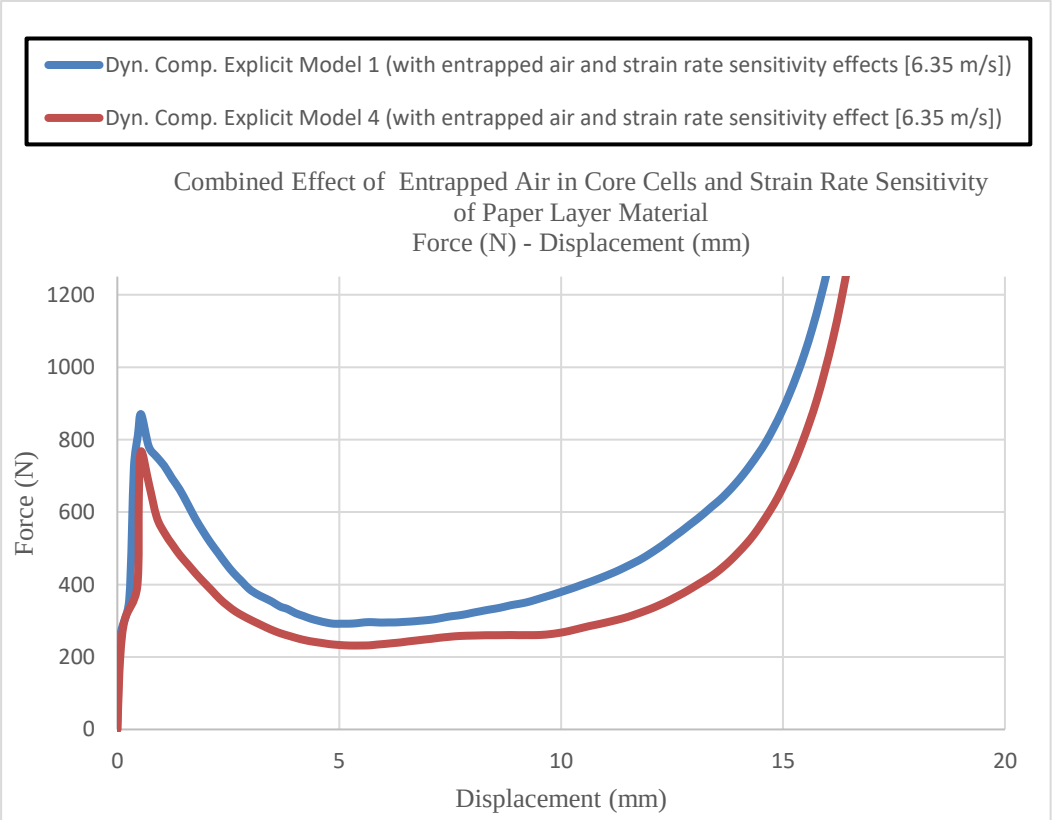

Figure 4.18. Comparison of explicit model 1 and explicit model 4 results.

When the model results were examined, it was seen that the entrapped air, strain rate sensitivity and micro-inertia affected the dynamic compressive behavior of the paper-based honeycomb structure at different contribution rates. In order to investigate at which deformation stage these effects are more effective, different data points were selected in the model and test curves and the force increase percentages at these points were calculated. The calculation results are given in Figure 4.19 with absolute scale.

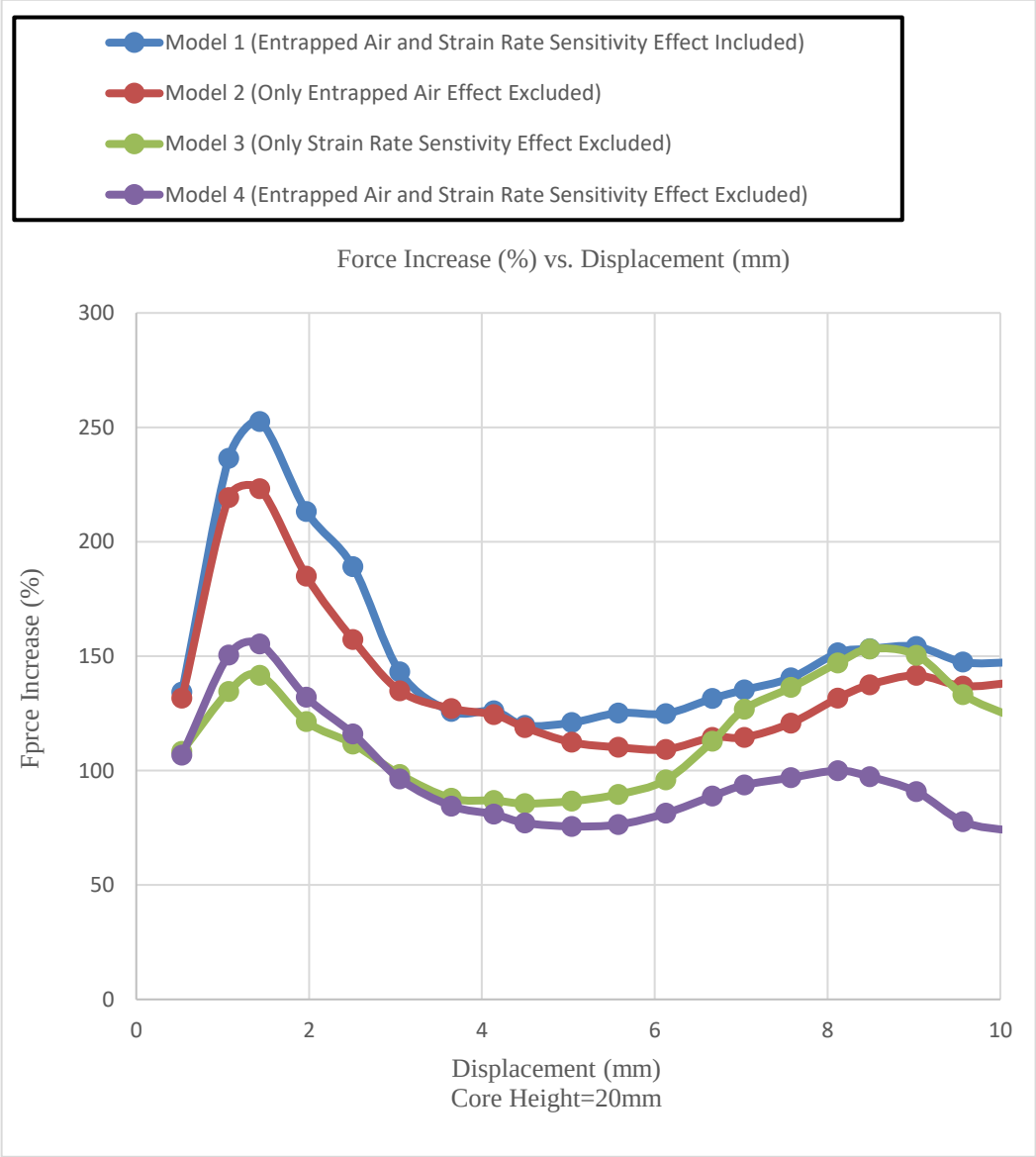

Figure 4.19. Force Increase Percentage

As it can be clearly seen, the force increase values measured in the elastic-plasticity region are higher than the increase values measured at the peak force point.

Therefore, it was concluded that the dynamic response of the structure was higher in the pre-plateau region.

When the model results are evaluated separately, the contribution of the effects to the increase in force values can be examined in more detail. It is seen that the contribution of the strain rate sensitivity effect on the dynamic compressive behavior is more significant in the comparison of the model 2 curve, in which the air effect is neglected, and the model 3 curve, where the strain rate effect is neglected.

In the curve of model 4, in which both effects are neglected, it is seen that the strength increase values before the plateau region are higher than the strength increase values measured in model 3, where only the entrapped air effect is included. The reason for this can be explained as the escaping of entrapped air, causing separation of the double-thickness walls, thus reducing the force for a short time. After the continued folding movement, the air was entrapped again and causing an increase in the force values in the plateau region.

CHAPTER 5

CONCLUSION

As mentioned in the previous sections, many studies have been carried out on the dynamic and quasi-static compressive behavior of paper-based honeycomb structures, which is widely used in all industries. As a result of the studies carried out within the scope of this thesis, detailed information was obtained about the compressive behavior of the paper-based honeycomb, especially under dynamic loads. Moreover, a micro-mechanical numerical model was developed that includes all the geometrical details of the honeycomb structure and the entrapped air inside the core cells. The developed modelling method is suitable for use in further studies to optimize the geometric parameters of the honeycomb structure. The cushioning performance of core types under dynamic and quasi-static loads can be predicted using this method at the design stage without the need for experimental study. Effective use of FE tools can help to find the most suitable core design for the requirements by reducing the cost and labor required for experimental studies.

The main findings of this study:

In the tensile test results of the paper strips specimens prepared in the MD and CD directions, it was observed that the paper exhibited an orthotropic behavior as expected. Since only the compression behavior in the through thickness direction was investigated in the numerical models in the study, this effect was neglected. However, it is predicted that the orthotropic structure of the paper will affect behavior of the honeycomb structure in in-plane, oblique and shear loading conditions.

All tests were carried out under controlled temperature and relative humidity. However, studies in the literature show that the strength of paper-based materials decreases due to the breaking of cellulose chains with increasing humidity. For this reason, environmental conditions should be taken into account in the characterization study of paper-based honeycomb structures.

The ASTM standard clearly states that the number of cells within the specimen planform area will affect the test results. Verifying the usability of the test specimens that will be used in non-standard test systems such as the Direct Impact by comparing them

with the test specimens conforming to the standards will increase the reliability of the result. As mentioned in chapter two, quasi-static compression test was performed with square and circular specimens. Since there was no significant difference between the test results, it was decided to use circular specimens.

In comparison of dynamic and quasi-static compression test results, an average increase in force of 136.19% was observed. This means that the structure under dynamic load will exhibit a stiffer behavior. The quasi-static crushing limit values are usually shared in the product data sheets provided by the suppliers. Although the calculations made with these limit values give good results in conditions such as stacking, in cases such as drop, the honeycomb structure will behave stiffer than expected and transfer the impact energy to the object that needs to be protected. Since the damage to the object will mean the failure of the packaging system, the dynamic compressive behavior of honeycomb structures should be considered in the design of packaging systems that will be subjected to dynamic loads.

A series of numerical modeling studies were carried out to further investigate the dynamic and quasi-static compressive behavior of paper-based honeycombs. Implicit models were established for modeling of quasi-static compression tests, and explicit models were established for modeling of dynamic compression tests. Force-displacement curves obtained from experimental studies were used for validation of numerical models. In the validation study, the numerical model results showed good correlation with the test results. While the difference between dynamic compression test and explicit model results is 8.67%, the difference between Quasi-static compression test and implicit model is 4.15%. A significant difference is observed between the numerical and experimental results in the transition values of the densification region. The main reason is that the core-face connections of the specimens can be separated or peeled during deformation, but the connection cannot be separated due to the TIED contact type, which provides a permanent contact between core-face connection in numerical models. This situation causes an additional constraint and leads to an increase in force values by locking the folding mechanism after 50% strain. For this reason, when examining the force increase values, the region before the densification limit was taken into account.

Using Ls-Dyna, the effects of entrapped air, strain rate sensitivity and micro-inertia on the dynamic compressive behavior of the paper-based honeycomb structure were investigated. When the results were examined, it was observed that the air trapped inside the cell had a contribution rate of 7.08%, and the strain rate sensitivity of the paper

layer material had a contribution rate of 18.02%. It has been observed that the strain rate sensitivity of the paper layer material is more effective than the entrapped air inside the core cells on dynamic compressive behavior of the paper-based honeycomb structure. The result of the explicit model, in which both entrapped air and strain rate sensitivity effects were neglected, was compared with the result of the implicit model, and the micro-inertia effect was examined. In the comparison of result curves, it was calculated that the micro-inertia effect caused approximately 96.56% increase in force values. It should be noted that when the entrapped air effect is included in the models, the air bursts the double-thickness walls as it escapes. The separation of double-thickness walls may affect the contribution rate of the micro-inertia effect. For this reason, the micro-inertia effect to be observed in the entrapped air effect included models may change depending on the deformation that will occur in the structure.

When the dynamic compression test model results were examined, it was seen that the entrapped air, strain rate sensitivity and micro-inertia affected the dynamic compressive behavior of the paper-based honeycomb structure at different contribution rates. In order to investigate at which deformation stage these effects are more effective, different data points were selected in the model result curves and the force increase percentages at these points were calculated. It was observed that the effects caused a significant increase in force values, especially in the elastic-plasticity region. This region includes the deformation mode extending from the initial folding of the cell walls to the plate region.

Further study recommendations:

Investigating the effect of temperature and moisture, orthotropic behavior of paper, different core types and different loading conditions (in-plane, shear, oblique) with experimental and numerical models will help one to understand the mechanical behavior of paper-based honeycomb structures.

REFERENCES

1. Aziz, M. S.; El sherif, A. Y. Biomimicry as an Approach for Bio-Inspired Structure with the Aid of Computation. *Alexandria Engineering Journal* **2016**, *55* (1), 707–714. https://doi.org/10.1016/j.aej.2015.10.015.

2. Benyus, J. M. *Biomimicry : Innovation Inspired by Nature*; Perennial: New York, Ny, 2002.

3. Lu, G.; Yu, T. X. *Energy Absorption of Structures and Materials*; Elsevier, 2003.

4. Mills, N. Finite Element Modelling of Foam Deformation. *Polymer Foams Handbook* **2007**, 115–145. https://doi.org/10.1016/b978-075068069-1/50007-6.

5. Reay, J. An Investigation into the Dynamic Response of Cardboard Honeycombs, University of Sheffield, 2014.

6. Wang, D.-M.; Wang, Z.-W. Experimental Investigation into the Cushioning Properties of Honeycomb Paperboard. *Packaging Technology and Science* **2008**, *21* (6), 309–316. https://doi.org/10.1002/pts.808.

7. Fayemi, P.-E.; Maranzana, N.; Bersano, G.; Aoussat, A. Bio-Inspired Design Characterisation and Its Links with Problem Solving Tools; 2014.

8. Tasdemirci, A.; Akbulut, E. F.; Guzel, E.; Tuzgel, F.; Yucesoy, A.; Sahin, S.; Guden, M. Crushing Behavior and Energy Absorption Performance of a Bio-Inspired Metallic Structure: Experimental and Numerical Study. *Thin-Walled Structures* **2018**, *131*, 547–555. https://doi.org/10.1016/j.tws.2018.07.051.

9. Aizenberg, J.; Weaver, J. C.; Thanawala, M. S.; Sundar, V. C.; Morse, D. E.; Fratzl, P. Skeleton of *Euplectella* Sp.: Structural Hierarchy from the Nanoscale to the Macroscale. *Science* **2005**, *309* (5732), 275–278. https://doi.org/10.1126/science.1112255.

10. Wang, Z.-W.; E, Y. P. Mathematical Modelling of Energy Absorption Property for Paper Honeycomb in Various Ambient Humidities. *Materials & Design* **2010**, *31* (9), 4321–4328. https://doi.org/10.1016/j.matdes.2010.03.053.

11. Gibson, L. J.; Ashby, M. F. *Cellular Solids*; Cambridge University Press, 1999.

12. Lu, L.-X.; Sun, Y.-P.; Wang, Z.-W. Critical Buckling Load of Paper Honeycomb under Out-of-Plane Pressure. *Packaging Technology and Science* **2005**, *18* (3), 141–150. https://doi.org/10.1002/pts.683.

13. Wang, D.-M.; Wang, Z.-W. Experimental Investigation into the Cushioning Properties of Honeycomb Paperboard. *Packaging Technology and Science* **2008**, *21* (6), 309–316. https://doi.org/10.1002/pts.808.

14. Aminanda, Y.; Castanié, B.; Barrau, J.-J. .; Thevenet, P. Experimental Analysis and Modeling of the Crushing of Honeycomb Cores. *Applied Composite Materials* **2005**, *12* (3-4), 213–227. https://doi.org/10.1007/s10443-005-1125-3.

15. Wang, D.-M.; Wang, Z.-W.; Liao, Q.-H. Energy Absorption Diagrams of Paper Honeycomb Sandwich Structures. *Packaging Technology and Science* **2009** , *22* (2), 63–67. https://doi.org/10.1002/pts.818.

16. E, Y.-P.; Wang, Z.-W. Effect of Relative Humidity on Energy Absorption Properties of Honeycomb Paperboards. *Packaging Technology and Science* **2010**, *23* (8), 471–483. https://doi.org/10.1002/pts.912.

17. Wu, E.; Jiang, W.-S. Axial Crush of Metallic Honeycombs. *International Journal of Impact Engineering* **1997**, *19* (5-6), 439–456. https://doi.org/10.1016/s0734-743x(97)00004-3.

18. Zhao, H.; Gary, G. Crushing Behaviour of Aluminium Honeycombs under Impact Loading. *International Journal of Impact Engineering* **1998**, *21* (10), 827–836. https://doi.org/10.1016/s0734-743x(98)00034-7.

19. Zhao, H.; Elnasri, I.; Abdennadher, S. An Experimental Study on the Behaviour under Impact Loading of Metallic Cellular Materials. *International Journal of Mechanical Sciences* **2005**, *47* (4-5), 757–774. https://doi.org/10.1016/j.ijmecsci.2004.12.012.

20. Yamashita, M.; Gotoh, M. Impact Behavior of Honeycomb Structures with Various Cell Specifications—Numerical Simulation and Experiment. *International Journal of Impact Engineering* **2005**, *32* (1-4), 618–630. https://doi.org/10.1016/j.ijimpeng.2004.09.001.

21. Smithson, G. *Energy Dissipation Characteristics of Air-Drop Materials under Impact Loading*; Tech. rep. Lowell Technological Institute Research Foundation, 1957.

22. Ripperger, E. A.; Briggs, W. R. *Variations in the Crushing Strength of Paper Honeycomb*; The University of Texas: Austin, Texas: Engineering Mechanics Research Laboratory, 1969.

23. Ripperger, E. A.; Briggs, W. R. *The Crushing Strength of Paper Honeycomb*; The University of Texas: Austin, Texas: Engineering Mechanics Research Laboratory, 1973.

24. Guo, Y.; Zhang, J. Shock Absorbing Characteristics and Vibration Transmissibility of Honeycomb Paperboard. *Shock and Vibration* **2004**, *11* (5-6), 521–531. https://doi.org/10.1155/2004/936804.

25. Wang, D. Impact Behavior and Energy Absorption of Paper Honeycomb Sandwich Panels. *International Journal of Impact Engineering* **2009**, *36* (1), 110–114. https://doi.org/10.1016/j.ijimpeng.2008.03.002.

26. Baum, G. A.; Habeger, C. C.; Fleischman, E. H. Measurement of the Orthotropic Elastic Constants of Paper. *smartech.gatech.edu* **1982**.

27. Mäkelä, P.; Östlund, S. Orthotropic Elastic–Plastic Material Model for Paper Materials. *International Journal of Solids and Structures* **2003**, *40* (21), 5599–5620. https://doi.org/10.1016/s0020-7683(03)00318-4.

28. Castro, J. Elasto-Plasticity of Paper. *International Journal of Plasticity* **2003**, *19* (12),2083–2098. https://doi.org/10.1016/s0749-6419(03)00060-3.

29. Allaoui, S.; Aboura, Z.; Benzeggagh, M. L. Phenomena Governing Uni-Axial Tensile Behaviour of Paperboard and Corrugated Cardboard. *Composite Structures* **2009**, *87* (1),80–92. https://doi.org/10.1016/j.compstruct.2008.01.001.

30. Godshall, W. D. *Dynamic Tension Testing Equipment for Paperboard and Corrugated Fiberboard*; U.S. Dept. of Agriculture, Forest Service, Forest Products Laboratory: Madison, WI, 1965.

31. Song, B.; Chen, W. W. Split Hopkinson Pressure Bar Techniques for Characterizing Soft Materials. *Latin American Journal of Solids and Structures* **2005**.

32. Flanagan, D. P.; Belytschko, T. A Uniform Strain Hexahedron and Quadrilateral with Orthogonal Hourglass Control. *International Journal for Numerical Methods in Engineering* **1981**, *17* (5), 679–706. https://doi.org/10.1002/nme.1620170504.

33. Lurie-Luke, E. Product and Technology Innovation: What Can Biomimicry Inspire? *Biotechnology Advances* **2014**, *32* (8), 1494–1505. https://doi.org/10.1016/j.biotechadv.2014.10.002.

34. ASTM Standard ASTM D828-16e1, "Standard Test Method for Tensile Properties of Paper and Paperboard Using Constant-Rate-of-Elongation Apparatus" ASTM International, Book of Standards Volume: 10.01, www.astm.org

35. ASTM Standard ASTM C365/C365M-16, "Standard Test Method for Flatwise Compressive Properties of Sandwich Cores" ASTM International, Book of Standards Volume: 15.03, www.astm.org

36. Seven, S. B. The Development of a New Testing Methodology in Dynamic Mechanical Characterization of Concrete. M.Sc. Thesis, Izmir Institute of Technology, 2018.

37. LSTC. *Ls-Dyna Theory Manual*; Livermore Software Technology Corporation, 2016.

38. LSTC. *LS-DYNA Keyword User's Manual*; Livermore Software Technology Corporation, 2016; Vol. 1.

39. LSTC. *LS-DYNA Keyword User's Manual Material Models*; Livermore Software Technology Corporation, 2016; Vol. 2.

40. Schulgasser, K. The In-Plane Poisson Ratio of Paper. *Fibre Science and Technology* **1983**, *19* (4), 297–309. https://doi.org/10.1016/0015-0568(83)90015-5.

41. Szewczyk, W. Determination of Poissons Ratio in the Plane of the Paper. *Fibres & Textiles in eastern Europe* **2008**, *16.4*, 117–120.

42. ANSYS. *SpaceClaim User's Manual*; ANSYS, Inc., 2016.

43. Altair HyperWorks User's Manual; Altair Engineering Inc., 2021.

44. Côté, F.; Deshpande, V. S.; Fleck, N. A.; Evans, A. G. The Out-of-Plane Compressive Behavior of Metallic Honeycombs. *Materials Science and Engineering:A* **2004**, *380* (1-2),272–280. https://doi.org/10.1016/j.msea.2004.03.051.